Wind and Structures, *Vol. 30, No. 1 (2020) 99-117*
DOI: https://doi.org/10.12989/was.2020.30.1.099

Peak pressures on low rise buildings: CFD with LES versus full scale and wind tunnel measurements

Aly Mousaad Aly*[1] and Hamzeh Gol-Zaroudi [2a]

[1]*Winsdstorm Impach, Science and Engineering (WISE) Lab, Civil & Environmental Engineering, Louisiana State University, Baton Rouge, USA*
[2] *Windstorm Impact, Science and Engineering(WISE), Louisiana State University, Research & Modeling, AIR Worldwide, Boston, USA*

(Received August 24, 2018, Revised March 25, 2019, Accepted November 20, 2019)

Abstract. This paper focuses on the processes of wind flow in atmospheric boundary layer, to produce realistic full scale pressures for design of low-rise buildings. CFD with LES turbulence closure is implemented on a scale 1:1 prototype building. A proximity study was executed computationally in CFD with LES that suggests new recommendations on the computational domain size, in front of a building model, apart from common RANS-based guidelines (e.g., COST and AIJ). Our findings suggest a location of the test building, different from existing guidelines, and the inflow boundary proximity influences pressure correlation and reproduction of peak loads. The CFD LES results are compared to corresponding pressures from open jet, full scale, wind tunnel, and the ASCE 7-10 standard for roof Component & Cladding design. The CFD LES shows its adequacy to produce peak pressures/loads on buildings, in agreement with field pressures, due to its capabilities of reproducing the spectral contents of the inflow at 1:1 scale.

Keywords: Atmospheric Boundary Layer (ABL); building aerodynamics; wind loading correlation; turbulence; wind pressure measurement; Large Eddy Simulation (LES); vortex method; Component and Cladding (C&C) design; scale effects

1. Introduction

In most parts of the United States, especially in the east coast and the southern parts, it has yearly been widespread that hurricanes and severe windstorms hit and damage buildings. Considering the population growth in coastal areas, coastal zones are being more and more concentrated with residential buildings. These buildings are mostly light low-rise buildings constructed from wooden materials with a different aerodynamic performance compared to high-rise buildings. The majority of failures in low-rise buildings are reported because of strong wind effects on building's envelope and specifically on roof panels (He *et al.* 2017).

The performance of roofs in low-rise buildings can differ significantly during a windstorm according to the shape of roof and its dimension. In large roofs, the correlations between the pressure fluctuations acting on different parts of the roof are usually low. In addition, the possible effect of resonant response is anticipated to be substantial on large roofs (Holmes 2015). The roof components and claddings in small roofs are usually exposed to damage during the storm winds due to local fluctuating negative pressure (suction effects) from flow separation, which occurs at the edges and corners of the roof. Fig. 1 represents wind flow around a low-rise building (Holmes 2015). The flow is separating from the sharp edges on the roof surface and re-attaching again in a fluctuating manner within the separation zones at a distance that is called separation bubble length, causing suction effects on the roof surface. The stagnation point is also specified in the windward wall, where the along-wind velocity is zero.

Field measurements of wind loads on an open roof during Typhoons suggest that the non-Gaussianity of wind pressures leads to large pulses in the time-histories of measured data. The corresponding peak factors were estimated using classical methods (Feng *et al*. 2018). Since the past decades, wind tunnel modelling has been widely used as a generic technique in order to estimate wind loads on buildings. However, according to the literature, there is still a doubt in the wind engineering community regarding the adequacy of wind tunnels to predict exactly the full-scale measurements in real life. For instance, as described in (Simiu 2009), there were 50% differences between wind tunnel aerodynamic measurements at six reputable centers for roof corner pressure coefficients and peak wind-induced bending moment in structural frames of low-rise buildings. It is worthy to mention that the American Society of Civil Engineers (ASCE) 7-10 standard for wind loads on components and cladding (C&C) come basically from published wind tunnel test results. The recent failures in solar panels and low-rise buildings during hurricanes and high winds prove that the peak pressures are not well addressed in code-specified design recommendations. Therefore, investigations shall be carried out to come up with alternative tools for a proper flow simulation in accordance to the real-world ABL winds, to fill this gap in available design standards (Aly 2014). Simulation of wind flow around a low-rise building is considered as a bluff body aerodynamic problem which deals with modelling complex spatial and temporal turbulence structures. This complexity mainly comes from the transient nature of

*Corresponding author, Ph.D.
E-mail: aly@LSU.edu
[2a] Ph.D.

ISSN: 1226-6116 (Print), 1598-6225 (Online)

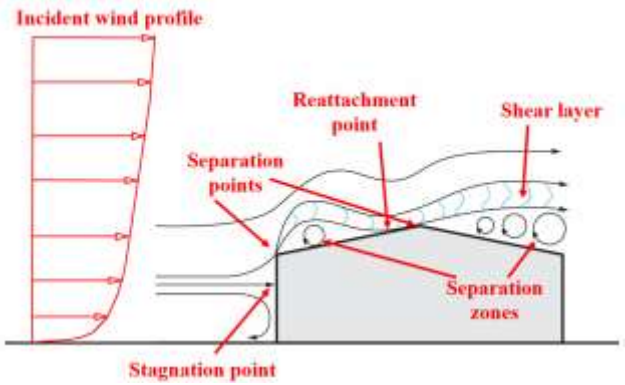

Fig. 1 Wind flow around a low-rise building: representing fluctuating flow separation and re-attachment (adopted from (Simiu 2011)

incident turbulent flows, and the fluctuating pattern of flows near the separation points.

To address these issues, in this paper, Computational Fluid Dynamics (CFD) tools with Large Eddy Simulation (LES) turbulence closure are implemented on a Texas Tech University (TTU) full-scale building model with appropriate inflow fluctuations to mimic peak pressures on the roof surfaces. CFD has received a renowned interest as a powerful tool to simulate wind flows and their impact on the infrastructure. CFD shows a promising potential when used to study the transient nature of wind flows (Yousef *et al.* 2018). The effect of dimensionality on the CFD results of turbulent flow around a bluff body was investigated in Ozdogan *et al.* (2017). 2D models yield agreeable results with 3D models, for various flow situations, when compared experimental data. Results show that the 3D CFD technique is an effective approach in the analysis of wind impact on complex-shaped structures (Moret Rodrigues *et al*. 2017). CFD modeling was used in integrated analysis for wind energy assessment, yielding comparable computational wind speed data to experimental results (Dhunny *et al.* 2015).

In this paper, the motivation is to reproduce peak pressures on the roof surface of low-rise buildings in CFD LES model by using appropriate inlet turbulence properties, and to investigate if the roof design peak pressure coefficients are correctly defined in ASCE 7-10 code. The vortex method is employed to generate the inflow wind fluctuations at the inlet boundaries for representing the real-world atmospheric boundary layer (ABL) wind characteristics by examining various sets of turbulence intensity (TI), and turbulence length scale (TLS). The CFD results are compared with a full-scale benchmark data from the Wind Engineering Research Field Laboratory (WERFL) at TTU as field measured wind pressure and velocity data. In addition, wind-tunnel measurements from the National Institute of Standards and Technology (NIST), and the University of Western Ontario (UWO), and open-jet testing at Louisiana State University (LSU) are compared with CFD LES results to investigate the scale effects. Eventually, the values of peak pressure coefficients are compared with external pressure coefficients, *GCp,* specified for components and cladding (C&C) in ASCE 7-10 to study how reliable those recommended design values are. In next sections, the details of the technique used for generating the inflow velocity fluctuations in CFD LES are presented.

2. Inflow velocity fluctuation

As CFD techniques have been developed over the recent years, LES becomes one of the widely used turbulence closure to simulate turbulent flows of engineering interests. However, one of the main challenges in computational wind engineering and using CFD simulations via LES turbulence closure is generating appropriate inflow fluctuation at the inlet that is representing the real-world ABL wind characteristics. If the inlet velocity boundary condition is not appropriately prescribed, the LES would require a high execution time to produce a fully developed turbulence. This fact is true even for a stationary turbulent flow. The current study is trying to address this issue by suggesting the best approach for generating inlet velocity fluctuations with tuned parameters and appropriate initial values using the available CFD tools.

According to the literature, over the past decade, several techniques were proposed for generating the inflow turbulence for LES. As a general classification, the following three concepts can be presented (Keating *et al*. 2004): (1) precursor simulation, (2) recycling method, and (3) synthetic turbulence. In the precursor method, the flow simulation of the target zone is performed within 2 separate steps. First, the incoming wind flow in upstream of the interested zone is simulated having the spatial and temporal correlation and turbulence characteristics and stored in a "library" or a database. As the second stage, the generated fluctuating turbulent velocities are introduced into the inlet boundary of the target zone. The main drawback of the precursor is the high computational cost associated with huge data storage demand. The recycling method, in contrast, divides the computational domain into the driver domain and the calculation domain, and the flow is recycled in the driver domain until the flow gains stable statistical properties. The flow characteristics are mapped within a plane and stored to be introduced as the inflow velocity for the calculation domain (Lund *et al*. 1998). One of the shortcomings of the recycling method is related to the dependence of the generated flow characteristics on the roughness elements implemented at the floor of the driver domain. However, recently some techniques were suggested to alleviate this issue (Aboshosha *et al.* 2015). In addition, the recycling method requires a high computational cost to run the driver domain.

The so-called synthesized turbulence method is another widely used approach to generate the transient velocity field for inlet. A random field of fluctuating velocities with temporal and spatial scales is superimposed on a pre-defined mean flow at inlet. Perturbations may be produced using several different ways, such as Fourier techniques, the Proper Orthogonal Decomposition (POD) analysis, digital filter based method, and vortex method (Tabor and Baba-Ahmadi 2010). In this study, however, the vortex method is utilized to generate the fluctuating wind velocity at inlet appropriate for LES and creating target turbulence content

suitable for ABL condition. The spectral synthesizer and vortex method will be described in detail in the following sub-sections.

Spectral synthesizer

The spectral synthesizer method is based on generating velocity fluctuation components. The random flow generation (RFG) technique used in this method was originally proposed by Kraichnan (Kramlich 1980) and modified by Smirnov *et al*. (2001). A method for generating synthesized inlet fluctuations was introduced by Davidson by using Fourier series (Davidson 2007, 2008). The main drawback of this approach is that the input wind should be simulated first, and then the generated time series need to be introduced to the CFD solver through a user-defined function which enables the software to read the input wind corresponding to each time step at various locations across the inlet. This process imposes a large amount of time to the solver to communicate and receive the initial values at the inlet boundary which adds up significant computational cost to the CFD simulation. This approach, however, was found useful for simulating peak wind loads on solar panels in (Aly 2016).

It is worth noting that the RFG method has been utilized in ANSYS FLUENT and is called Spectral Synthesizer. In the software, the number of Fourier harmonics is fixed to 100 (FLUENT 2015). The inlet velocity fluctuations are added to the mean specified velocity during the simulation. In this way, the cost of the computation is improved considerably. However, RFG generates divergent-free velocity field with Gaussian spectra. Unfortunately, the lower ABL winds represent turbulent spectra with different characteristics than the Gaussian spectra (Lumley and Panofsky 1964). Therefore, RFG approach is not implemented in this research study for generating the inlet transient velocity fields.

Vortex method

Vortex method is a 2D grid-free technique for generating time-dependent perturbations at the inlet by adding a fluctuating vorticity field to a specified mean velocity profile at inlet. The perturbation is added in a two-dimensional plane normal to the streamwise flow direction. This method was initially developed by Sergent(Sergent 2002) and adopted to the CFD ANSYS FLUENT software by Mathey *et al*. (2006b). The vortex method is mathematically modelled as follows (Mathey *et al.* 2006b)

$$\frac{\partial \omega}{\partial t} + (\vec{u}.\nabla)\omega = \nu \nabla^2 \omega \tag{1}$$

where υ is the kinematic viscosity. This equation can be solved by using a particle discretization and randomly convecting vortex points that carry information about the vorticity field. The amount of vorticity carried by a given particle ί can be simulated by the circulation Γί and an assumed spatial distribution of the vortex, η as follows

$$\omega(\vec{y}, t) = \sum_{i=1}^{N} \Gamma(\vec{y}_i(t))\eta(|\vec{y} - \vec{y}_i(t)|) \tag{2}$$

$$\Gamma_i(x, y) = 4\sqrt{\frac{\pi A k(x, y)}{3N[2\,ln(3) - 3\,ln(2)]}} \tag{3}$$

$$\eta(\vec{x}) = \frac{1}{2\pi\sigma^2}(2e^{-|x|^2/2\sigma^2} - 1)2e^{-|x|^2/2\sigma^2} \tag{4}$$

where Ɲ is the number of vortex points and A is the area of the inlet section; Ƙ stands for the turbulence kinetic energy. The circulation Γⁱ represents the fluctuation intensity which is a function of the local turbulence kinetic energy. The discretized velocity field is represented by

$$\vec{u}(\vec{x}) = \frac{1}{2\pi}\sum_{i=1}^{N} \Gamma_i \frac{((\vec{x}_i - \vec{x}) \times \vec{z})(1 - e^{|\vec{x} - \vec{x}'|^2/2\sigma^2})}{\left|\vec{x} - \vec{x}_i'\right|^2} \tag{5}$$

where $\vec{z}$ is the unit vector in the along-wind direction. The control over the size of a vortex particle is provided through a defined parameter, σ which can be estimated from the inlet profiles of mean turbulence kinetic energy and mean dissipation rate as follows

$$\sigma = \frac{ck^{3/2}}{2\varepsilon} \tag{6}$$

where □= 0.16. The calculated minimum value of σ is bounded by the local mesh size to make certain that the simulated vortex will always belong to the resolved turbulence scales. At each characteristic time scale τ, the sign of circulation of each simulated vortex is randomly altered. This time scale defines the time required for a 2D vortex that is convected at inlet in the normal direction of the boundary and travels along n times its mean characteristic 2D size (σ_m), in a way that$n$ is fixed to a value of 100 from numerical testing.

It is worth noting that the vortex method only considers velocity fluctuations in the plane normal to the along-wing direction. However, ANSYS FLUENT benefits from a simplified linear kinematic model (LKM) that mimics the influence of the two-dimensional vortex in the along-wind mean velocity field (Mathey *et al.* 2006a). If the mean along-wind velocity U is considered as a passive scalar, the fluctuation $\boldsymbol{u'}$ resulting from the transport of $\boldsymbol{U}$ by the planar fluctuating velocity field $\boldsymbol{V'}$ is modeled by

$$u' = -\vec{v}'.\vec{g} \tag{7}$$

where $\vec{g}$ stands for the unit vector aligned with the mean velocity gradient $\nabla\vec{U}$. A random perturbation can be considered in the case when the defined mean velocity gradient is equal to zero. In this study, vortex method is employed to generate the inflow wind fluctuation at inlet for LES representing the real-world ABL wind characteristics.

3. Full-scale field measurements for CFD validation

As described earlier, in this study, in order to make certain that the developed CFD model of a low-rise building and the inlet wind velocity fluctuations are in accordance with real world ABL characteristics, the full-scale

benchmark data from the WERFL at TTU are used as field measured wind pressure and velocity data. A similar validation was made for a comparison with simulation data collected in a large scale physical facility at the Insurance Institute for Business & Home Safety (IBHS) (Morrison *et al*. 2012). In addition, WERFL TTU data set was used for wind tunnel measurement validation in (Bienkiewicz and Ham 2003, Okada and Ha 1992, Tieleman *et al*. 2003, Xu 1995).

The WERFL experimental building is a full-scale test building with dimensions of 13.72 m × 9.14 m × 3.96 m (H/B = 0.43, D/B = 1.5) and a slope of ¼:12 (β = 1.19°) for the gable roof, located in an open exposure natural environment in Lubbock, Texas (Levitan and Mehta 1992a, b). Provided in a report, TTU released the time histories and summary statistics for 15-minute duration records with flow direction acting through a 160 ft high meteorological tower and then impinging on the WERFL test structure (Smith *et al*. 2017). The meteorological tower is a guyed lattice structure instrumented at 5 heights of 8 ft (2.44 m), 13 ft (3.96 m), 33 ft (10.06 m), 70 ft (21.34 m), and 160 ft (48.77 m), to measure wind speed and wind direction. A 30 Hz sampling rate was adopted for acquisition of meteorological wind velocity and pressure data. It means that for each 15 minute data acquisition duration, each channel recorded 27,000 samples. On the surfaces of the full-scale building, 204 pressure taps were instrumented to record time series of pressure data. In this study, the two selected TTU dataset (run names of 279 and 1912) for comparison of pressure distribution with CFD LES results are listed in Table 1. However, for comparison of peak non-dimensional pressure coefficients on the roof of TTU building with external pressure coefficients, GCp, specified for components and cladding (C&C) in ASCE 7-10, other wind directions (14 directions) provided in (Smith *et al*. 2017) and the database were processed and examined as well.

4. LSU open-jet testing

In addition to the full-scale field measured TTU data, in this paper, the pressure measurement results from a small scale model of TTU low-rise building conducted within the LSU open-jet facility (Aly and Gol-Zaroudi 2017) are used for a comparison with code-specified components and claddings GCp design values in ASCE 7-10. Consequently, two models of the TTU low-rise building having the same aspect ratio, but different scales of 1:15 and 1:22.3, were created and tested in an open-jet facility at LSU for 2 wind angles of attack (0° and 90°). The small-scale models were made of 2.5 mm and 5 mm thick sheets of acrylic plastic. Table 2 represents the details of LSU open-jet testing, including the experimental setup, and data acquisition. As a result, a test duration of 9 min was determined for the scale of 1:15, and a duration of 6 min for the scale of 1:22.3, corresponding to 1-hour duration in prototype case. The sampling frequency for the pressure measurements was 625 Hz, and for the velocity recording it was 1250 Hz. The pressure measurement results were compared with available wind-tunnel data from NIST/UWO (Ho *et al*. 2003). In (Gol-Zaroudi and Aly 2017), it was shown that the turbulence properties of the approaching flow, scale issue, and open-jet exit proximity effects could influence the flow pattern on the two models of low-rise buildings, and how the length of separation bubble could alter on the roof surface in the lab. The contributions of these parameters on the values of the fluctuating external pressure coefficients on the roof surface were also discussed in (Gol-Zaroudi and Aly 2017). It was concluded that for the scale models that are placed at a horizontal distance of 2.5 H from the exit of the open-jet (H is the total height of the wind field), the contours of mean and peak pressure coefficients were well consistent with the results of NIST/UWO. This good agreement was observed in both LSU scale models (1:15

Table 1 Summary statistics of wind flow characteristics for selected record from WERFL (Smith *et al*. 2017)

Mode number	Run name	Run date	Building position	Angle of attack	Wind azimuth angle	Mean wind speed, mph
1001.01a	279	1/9/2003	270	9.6672058	279.66721	18.13
1001.02a	1912	4/6/2003	285	351.7236	276.7236	19.97

Table 2 Details of LSU open-jet testing of scaled models of TTU low-rise building, experimental setup, and data acquisition

Model Scale	1:22.3	1:15
Model dimensions, w × l × h	0.41 m × 0.61 m × 0.18 m	0.61 m × 0.91 m × 0.26 m
Pressure sampling frequency	625 Hz	625 Hz
Number of taps	206	206
Reference open-jet wind speed	8 m/s	8 m/s
Velocity sampling frequency	1250 Hz	1250 Hz
Sampling time	6 min	9 min
Upstream exposure	open-terrain	open-terrain
Upstream terrain roughness, Z_o	0.01 m	0.01 m
Wind angles (deg.)	0, 90	0, 90

and 1:22.3). However, the model with the scale 1:15 was believed to be a better representative of aerodynamic characteristics of the target building based on the comparison of wind-induced mean and peak pressure coefficients measured in the open-jet facility and those from NIST/UWO model. Therefore, in this paper, the pressure measurement results of the 1:15 scaled model are used for further investigation and comparison with the code-specified GCp design values in ASCE 7-10 for components and claddings of low-rise buildings in next sections.

5. CFD LES flow simulation for empty domain

In this study, in order to simulate ABL wind characteristics, including mean wind velocity profile, turbulence intensity and the appropriate turbulence spectrum contents, first an empty domain without the low-rise building was modelled. The purpose was to update/expand the existing guidelines for the longitudinal extension of the domain in front of the building model via LES, while the other recommendations (e.g., COST and AIJ) are mainly based on the Reynolds Averaged Navier–Stokes equations (RANS) models. Once the best location is found, another computational domain is generated to include the low-rise building at the recommended location from the inlet boundary of the empty domain. Therefore, it can be assured that the reproduced peak pressure values on the roof of the target low-rise building are induced from the correct ABL wind characteristics. In addition, less computational cost would be required for simulating and validating wind characteristics within an empty domain, as the cell numbers are less than the domain with building included in the computational domain. In the following, the steps that are pursued for achieving the appropriate wind flow in accordance with ABL characteristics are described in detail.

Empty domain size and defined monitoring profiles

The overall size of the empty computational domain was determined based on the recommendations of the Architectural Institute of Japan (AIJ), the practical applications of CFD to pedestrian wind environment around buildings (Tominaga *et al*. 2008), and the European Cooperation in Science and Technology (COST) (Franke *et al*. 2011), and by considering the TTU building dimensions that will be placed inside the empty domain after the first validation step. Therefore, the empty computational domain has a length of [40 h + length of the building, or x = 170 m], width of [14 h + width of the building, or z = 64 m], and height equals to [8 h, or y = 32 m], where h, l, and w stand for height, length, and width of the target TTU full-scale low-rise building. It is worth noting that the recommendation of COST and AIJ are mainly based on the Reynolds Averaged Navier–Stokes equations (RANS) models and therefore need to be revisited for the LES model in this study.

A general view of the domain size can be seen in Fig. 2 which also represents how the monitoring points are defined at different heights across the centerline of the empty domain to record velocity time histories. As a result, flow development across the domain can be examined and important flow characteristics such as, mean velocity profiles, turbulence intensities, and turbulence spectrum, can be compared with theoretical values for ABL. The horizontal distance of each column of monitoring points from the inlet in Fig. 2 is represented in Table 3. In this table, h stands for the height of the target low-rise building (h ≈ 4 m).

In order to perform a mesh sensitivity analysis for the empty computational domain, four different mesh sizes are defined as the details of refinements are listed in Table 4. The mesh cases are produced by using blockMesh utility in OpenFoam. For the length and width, uniform interval is used for meshing the domain. In all four mesh cases in Table 4, an expansion ratio of 4 was considered for the altitude (Y) direction. Finally, the mesh ID 2 was selected as the background blockMesh for the next step to create a high-quality mesh around the building model. Fig. 3 represents a 3D general view of the empty domain with a refine mesh of 1,036,800 cells created by blockMesh utility in OpenFOAM, and the assigned boundary conditions. As can be seen in Fig. 3, for the top, front wall and back wall, a "symmetry" boundary condition; for the bottom (ground) a "no-slip wall" was selected; for the outlet, an "outflow", and for the inlet a "velocity inlet" were assigned. For the inlet boundary, the mean wind velocity profile is introduced to the software by developing a User Defined Function (UDF) according to the log-law wind profile (Holmes

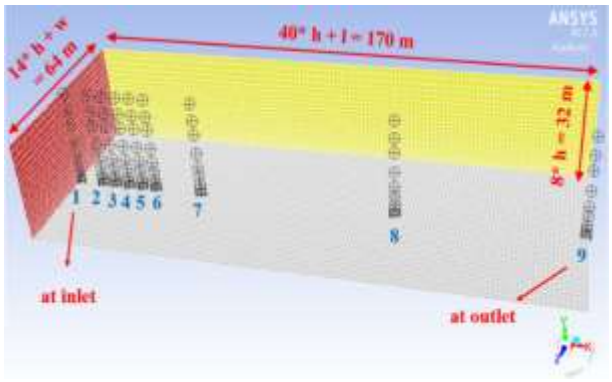

Fig. 2 The size of the empty domain (h, l, and w stand for height, length, and width of the target TTU low-rise building) and the monitoring points defined at different heights across the centerline of the empty domain to record velocity time histories

Table 3 Horizontal distance of each points from the inlet (h ≈ 4 m)

Points label	1	2	3	4	5	6	7	8	9
Distance from Inlet	1 m (0.25 h)	10 m (2.5 h)	15 m (3.75 h)	20 m (5 h)	25 m (6.25 h)	30 m (7.5 h)	46.5 m (11.63 h)	108.25 m (27 h)	170 m (42.5 h)

Table 4 Various cases created by using blockMesh utility in OpenFOAM to perform mesh sensitivity analysis

Mesh ID	Number of refinement in main directions			Cell numbers
	Length (x)	Width (z)	Height (y)	
1 (coarse)	128	48	24	147,456
2	170	64	32	348,160
3	221	84	42	779,688
4 (fine)	255	96	48	1,036,800

Table 5 Parameters used to define the inlet mean wind profile to the CFD solver

Parameter	$\bar{U}$ [m/s]	z_0 [m]	u^* [m/s]	z_{ref} [m]
Value	8.05	0.01	0.5383	3.96

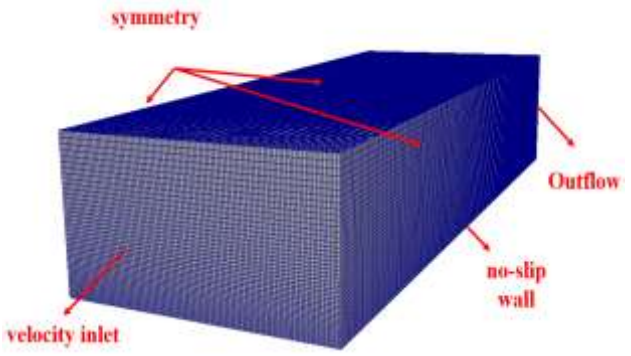

Fig. 3 A 3D general view of the empty domain with a refine mesh of 1,036,800 cells created by blockMesh utility in OpenFOAM, and the assigned boundary conditions

2015). The parameters used for inlet wind flow are represented in Table 5. The fluctuation of wind velocity at each time step is then generated by utilizing the vortex method by adding a fluctuating vorticity field to the specified mean velocity profile at the inlet boundary. It is worth noting that the mean wind velocity of 8.05 m/s at roof height is chosen based on the TTU (R279) mean wind velocity data at roof elevation.

In fluid flow simulations, the fidelity of numerical solutions is significantly affected by the near-wall modeling. In the near-wall regions, large gradients are observed in the solution variables. In real world problems, the ground surface is usually covered with natural elements such as: vegetation, soil, sand and rocks, and in some cases water surfaces. In CFD simulations, however, it is impossible to directly model every detail of the roughness elements with a refined mesh (Zhang 2009). Instead, the effect of near-wall regions shall be represented by near wall treatment functions. In ANSYS FLUENT, several wall functions are defined (FLUENT 2015). In this research study, the standard LES near wall treatment was used as a default option in ANSYS FLUENT for near wall treatment. In this case, the wall-function formulation depends on near wall mesh size. When the mesh is fine enough to resolve the laminar sublayer (typically with the first near-wall node placed at), the wall shear stress is obtained from the laminar stress-strain relationship

$$\frac{\bar{u}}{u_\tau} = \frac{\rho u_\tau y}{\mu} \tag{8}$$

When the mesh is too coarse to resolve the laminar sublayer, the law-of-the-wall is employed

$$\frac{\bar{u}}{u_\tau} = \frac{1}{\kappa} ln\, E\, (\frac{\rho u_\tau y}{\mu}) \tag{9}$$

where k is the von Kármán constant and E = 9.793.

6. Results of empty domain flow simulation

In this section, the results of CFD LES of the empty domain without the target low-rise building are presented, and the flow characteristics were examined at various heights along the centerline of the empty domain. The purpose, as described in earlier sections, is to define the best location within the computational domain that the wind characteristics are in good agreements with ABL theoretical values and field measurements for open-terrain condition from the WERFL at TTU. The time histories of wind velocity components are stored during the simulation at each monitoring points which are depicted in Fig. 2. The data were analyzed by extracting the mean velocities and turbulence intensities at each point to create the corresponding CFD LES profiles and are compared with theoretical values and full-scale measurements. Turbulence spectrums are also calculated at desirable heights within the target location from the inlet boundaries. The results are described in detail in next sub-sections as follows.

Tuning the input parameters for vortex method

In ANSYS FLUENT in order to define the transient nature of wind velocity, a fluctuating vorticity field will be added to a specified mean velocity profile at inlet boundary. There are two parameters that can be assigned as inputs to control the quality of turbulence structure of the velocity field which are (1) turbulence intensity (TI), and (2) turbulence length scale (TLS). These inputs are assumed as averaged over the height of inlet domain, and the software after introducing the mean wind velocity profile according to the log-law wind profile to the software by using a UDF, the other two parameters of TI, and TLS should be trialed to find the best set of tuned parameters that can mimic desired only accepts one single entry for each parameter. Therefore, ABL wind characteristics. Fig. 4 represents the results of several trials with various values for TI and TLS for inlet at roof height of 3.96 m with a target theoretical TI of 16.9% (TI_{target} = 16.9%). After examining several sets of input, it was observed that the value of TI should be higher at inlet boundary to reproduce a desirable level of turbulence at the target location along the computational domain after the inlet.

According to Fig. 4, the case with TI = 25% and TLS = 10 m resulted a good match for turbulence intensity at roof height at location 3. To fully check the properties of flow

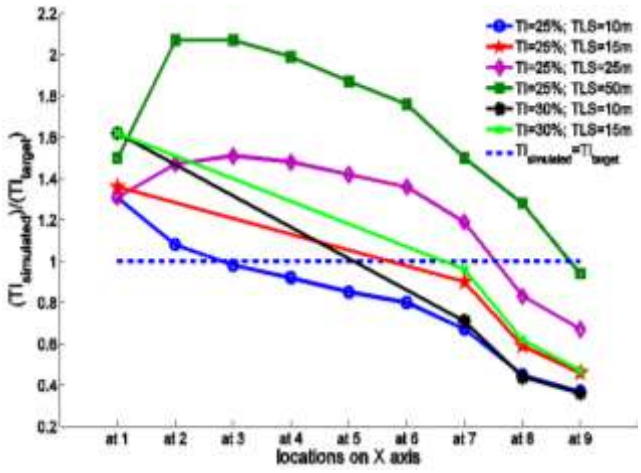

Fig. 4 The results of several trials for various sets of inputs in terms of turbulence intensity (TI) and turbulence length scale (TLS) for inlet at roof height of 3.96 m with a target theoretical TI of 16.9%

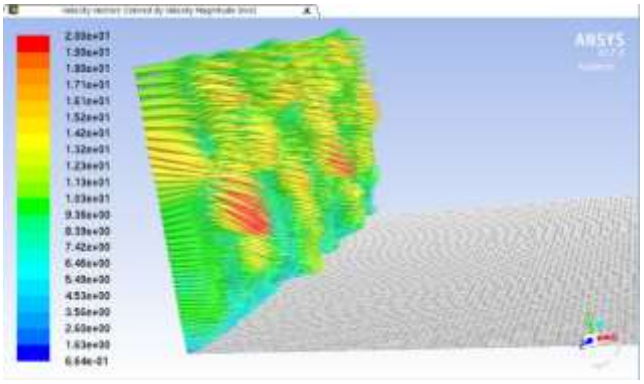

Fig. 5 The LES simulated instantaneous velocity vectors at inlet boundary colored by velocity magnitude (m/s) for the empty domain with fine mesh and input variables of TI = 25% & TLS = 10 m

for this set of inputs, the results of flow simulation for this case are further investigated within the next sections. In addition, at location 7, the case with TI = 30% and TLS = 15 m, yielded a good agreement with the target TI. Therefore, these two locations (locations 3 and 7) are selected as the recommended locations of testing for building model within the next sections to investigate the effects of the simulated flow characteristics to reproduce the pressure distribution on the roof surface. It should be noted that even though Fig. 4 shows the turbulence intensity of TI = 25% and TLS = 10 m at location 7 is not as perfect as the other two cases, it was selected as a CFD run case to check how the inflow boundary proximity has an effect on the spatial correlation of the wind pressure coefficients and the reproduction of peak pressure values on the roof surface. This will be further discussed in the following sections.

Mean wind velocity profiles and turbulence characteristics

Fig. 5 represents the simulated instantaneous velocity vectors at inlet boundary colored by velocity magnitude

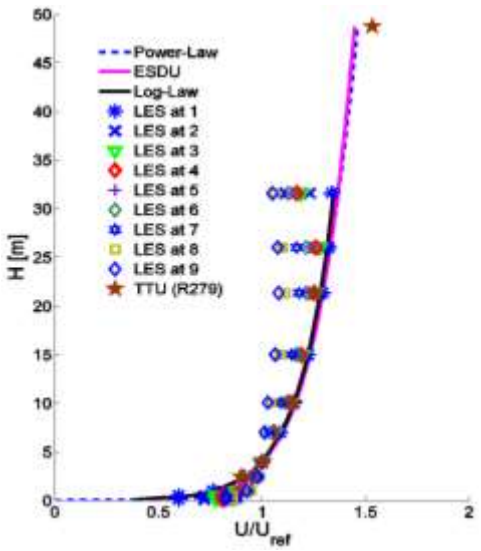

Fig. 6 CFD LES mean wind velocity profiles at various locations from inlet boundary along with the theoretical profiles for input variables of TI = 25% & TLS = 10 m

(m/s) for the empty domain with fine mesh and input variables of TI = 25% and TLS = 10 m. It shows how the fluctuating vorticity fields are added to the log-law mean velocity profile at inlet. Fig. 6 shows the mean along-wind velocity obtained at locations 1, 2, 3, 4, 5, 6, 7, 8, and 9 with the distances from the inlet defined in Table 3. It can be seen that by increasing the distance from the inlet, the simulated profiles are deviating from the target theoretical profile calculated by the power-law, log-law, and ESDU for the open-terrain condition (α was considered 0.15, and z_0 was selected 0.01 m for open terrain condition according to (Holmes 2015)). However, at location 1, 2, 3, and 4, the LES simulated wind velocity data is consistent with theoretical wind profiles specifically in lower parts of the profile. It proves that the LES turbulence closure can properly predict the flow velocity gradient. Fig. 7(a) represents the time history of along-wind velocity from the TTU field measurements. Fig. 7(b) shows the corresponding time history from CFD LES (TI = 25%, and TLS = 10 m) at roof height (3.96 m) at location 3 which is depicted in Fig. 2, and close to the inlet boundaries. The time history is reproduced for 15 min in real life to be comparable with the full-scale data. The velocity is changing over time around the mean velocity of 8.05 m/s.

The variation of the wind velocity over time are examined by calculating the turbulence intensity at each monitoring points along the computational domain in Fig. 8. The turbulence intensity profiles at different distances are showing a wider range. For instance, at location 1, very close to the inlet, the flow possesses a higher level of turbulence than the theoretical ones, and turbulence intensity is significantly decreasing at outlet boundaries at location 9. It shows how the turbulence of approaching flow within the domain can be changed over the distances from the inlet boundaries. It is also noticeable that at location 2, 3, and 4, the simulated LES profiles are following the theoretical profiles very well, and the LES turbulence closure with tuned parameters is able to properly replicate

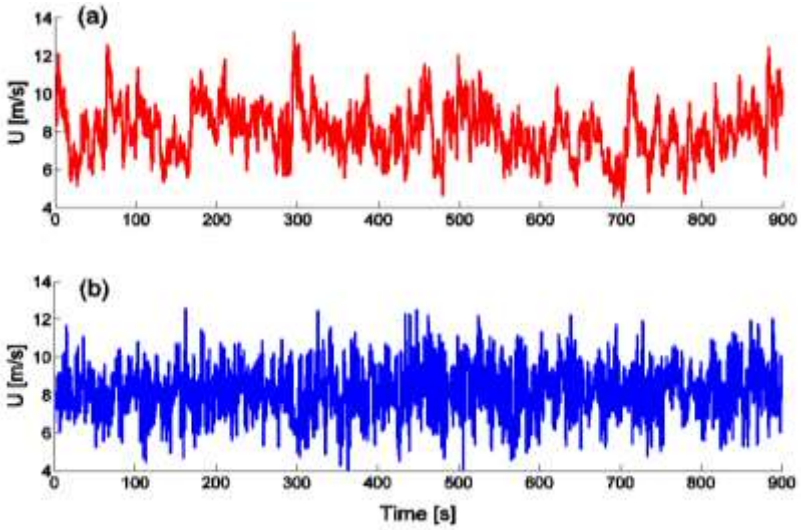

Fig. 7 Time history of along-wind velocity at roof height; (a) TTU field measurements (R279); (b) CFD LES at location 3 and TI = 25%, and TLS = 10 m as input variables

near-surface ABL profiles and turbulence intensities suitable to the real conditions of open-terrain. It should be noted that the demonstration of TI profiles in Fig. 8 is related to the flow with input variables of TI = 25% and TLS = 10 m, and for the other flow with input variables of TI = 30% and TLS = 15 m, at location 7 the simulated TI profile was also matching well with ABL wind. Therefore, the two simulated flow cases will be further investigated for testing the TTU building model at locations 3 and 7 in the following sections.

Spectral challenge

Fig. 9 represents the along-wind velocity spectrum for the LES simulated velocity data for input variables of TI = 25% and TLS = 10 m. These spectrums are calculated at roof reference height for various distances from t. inlet boundaries to check the energy distribution in different frequency ranges. The counterpart spectrums related to the TTU full-scale data for R279 and R1912 as described in Table 1, are also depicted in the Fig. 9. Because the CFD model was created with full-scale dimensions, there was no issue with time scale and velocity scale, and the simulated LES data were corresponding to 15 min in real life winds. The Kaimal and the ESDU spectrums are calculated according to the theoretical formulations and plotted in Fig. 9. It can be seen that the simulated LES spectrum is matching reasonable at high frequency with the two cases from TTU field measurements. As discussed in previous chapters, the high frequency parts of the spectrum are responsible for small scale eddies. However, discrepancies between the TTU field measurements and the simulated LES spectrums exist at frequencies. From the Fig. 9, it seems that the LES model is injecting higher energy at low-frequency part of the spectrum to the velocity field. However, the effect of the simulated LES spectrum on pressure distribution on the roof of a low-rise building will be investigated in the next section. It is worth noting that even the full-scale field measured winds did not follow the theoretical spectrums in Fig. 9, and even the two Kaimal

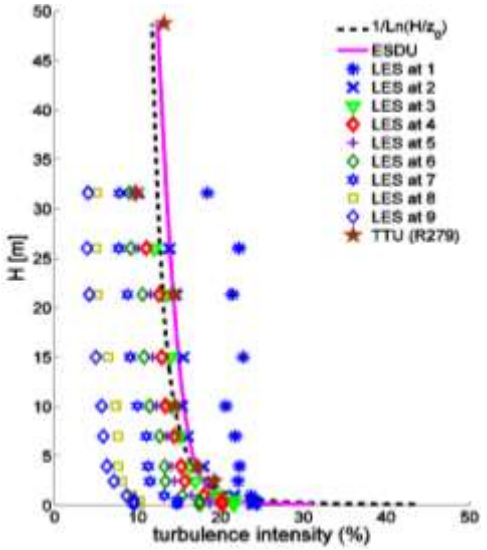

Fig. 8 CFD LES turbulence intensity (TI) profiles at various locations from inlet boundary along with the theoretical profiles for input variables of TI = 25% & TLS = 10 m

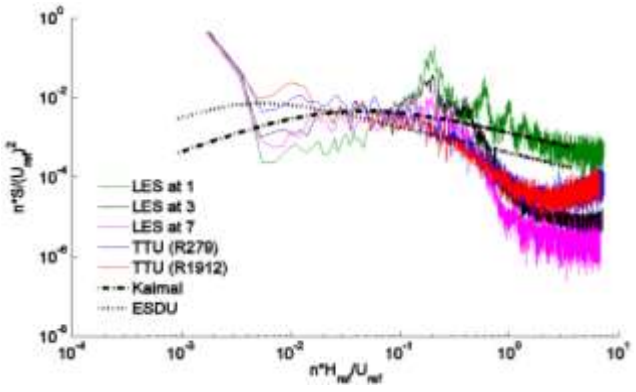

Fig. 9 Along-wind velocity spectrum at roof height (h = 3.96 m) for LES input variables of TI = 25% & TLS = 10 m, along with theoretical profiles, and two cases from TTU

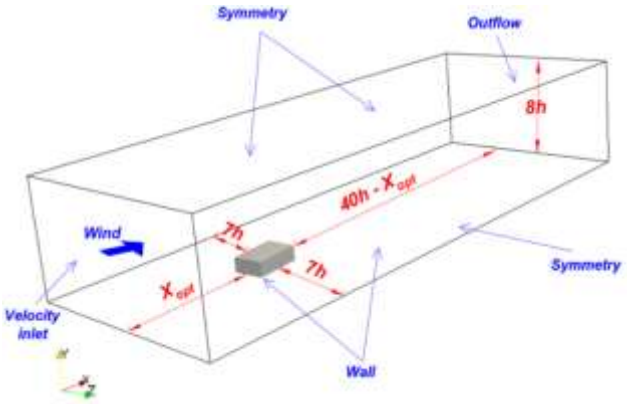

Fig. 10 Computational domain size and the boundary conditions (h is the height of the building); the building is rotated 9.67 degrees in accordance to its longitudinal axis

and ESDU are not following exactly each other. This discrepancy was also reported in (Mann 2012, Mann *et al*. 1998). It is believed to be due to the larger along-wind velocity length scales assumed by ESDU which was supported by (Højstrup *et al*. 1990). It emphasizes the fact that reproducing the spectrum contents is still a major challenge and an open area for research in the wind engineering community in which discrepancies in pressure measurements can be referred to this issue.

7. Main computational domain including building

After examining the flow characteristics at various locations inside the empty computational domain, the two locations (locations 3 and 7 in Fig. 2) for placing the low-rise building inside the computational domain were determined accordingly. In this section, the procedure to model the low-rise building within the computational domain are presented.

Computational domain size

As described earlier, the computational domain size was determined based on the recommendations of the Architectural Institute of Japan (AIJ), the practical applications of CFD to pedestrian wind environment around buildings (Tominaga *et al.* 2008), and the European Cooperation in Science and Technology (COST) (Franke *et al.* 2011). The guidelines proposed by COST mainly consist of results obtained from a literature review, while the AIJ recommendations are mainly derived from a lot of wind tunnel experiments, field measurements and computations using different CFD codes. Based on the COST and AIJ, the distance between the inflow boundary and the building for a single building was recommended 5 h (h is the mean roof height) if the approach flow profiles are well known. COST cited some research studies that recommended 8 h for this distance. According to the COST, this distance is advised, even a larger distance if the approaching flow profiles are not available to allow for a realistic flow establishment. COST recommends that the outflow boundary can be positioned at least 15 h behind the building to permit the flow re-develop behind the wake region. However, the recommendations of both COST and AIJ are mainly based on the Reynolds Averaged Navier–Stokes equations (RANS) models and therefore need to be revisited for the LES model in this study. In contrary to the COST recommendations, VDI (the German Association of Engineers) suggests blockage and building type dependent distances (VDI 2005). For a single building with low blockage ratio, a distance of 2 h is recommended from the inlet boundary. For larger blockage ratio (for instance 10%), a distance of 8 h is recommended. It can be concluded that there is a large range of recommended values concerning the longitudinal extension of the domain in front of the building model. In addition, those recommendations are not based on LES results. Therefore, in this study, it is aimed to investigate the influence of inflow boundary proximity for a low-rise building via LES and to update/expand the existing guidelines (e.g., COST and AIJ) for longitudinal extension of the domain in front of the building in such a way to reasonably simulate ABL wind characteristics and reproduce the peak pressures on roof areas.

The computational domain in this study is represented in Fig. 10. As can be seen in Fig. 10, the top of the 3D computational domain is set at 8 h. The lateral boundaries are set at a distance of 7 h. This provides a blockage ratio less than 3% that is defined in (Franke *et al.* 2011) as the maximum allowable blockage ratio. The inlet boundary is set at a distance of X_{opt}. This distance was determined after the proximity sensitivity analysis which was performed in previous sections. It was shown that the flow characteristics at location 3 (X_{opt} = 3.75 h) and at location 7 (X_{opt} = 11.63 h) are in a better agreement with the theoretical profiles by applying two different sets of inputs for inlet flow. Testing building at these locations assures that the fluctuating inlet wind velocity possesses the necessary turbulent content representing the atmospheric boundary layer at the building location. Finally, the outlet boundary was set a distance of 40h-X downstream of the low-rise building location to allow developing the wake flow.

Computational mesh generation in OpenFOAM

In this study, to benefit from an open-source free software, and to apply a systematic approach, the OpenFOAM CFD package was used to create several mesh files by utilizing the SnappyHexMesh tool. The SnappyHexMesh is an automatic 3D hex-dominant mesh generation utility (OpenFOAM 2015) that helped to considerably save time in the meshing process in this study. The procedure to create the mesh is that first, the geometry of the full-scale TTU building was created in AutoCAD and then exported as Stereolithography (.stl) format. The '. stl' file was put in constant/triSurface directory as the input for building surface. Then SnappyHexMesh utility was implemented and run in parallel on LSU Mike-II High Performance Computing (HPC) clusters. The meshing procedure starts by defining a background mesh made of hexahedra using blockMesh utility, and then two phases of CastellatedMesh and SnapMesh will be proceeded for refinement and mesh morphing. The mesh refinement process can be controlled by commands written in snappyHexMeshDict dictionary file in the system folder. The SnappyHexMesh utility allows to define independent refinement boxes around the objects. This approach is an effective way for dealing with complex shapes with sharp edges to create high quality structured meshes. More details

Table 6 Various mesh cases created by using SnappyHexMesh utility in OpenFOAM to perform sensitivity analysis for the building included in the computational domain

Mesh ID	Cell numbers
1 (coarse)	340,000
2	768,000
3	1,700,000
4 (fine)	2,491,000

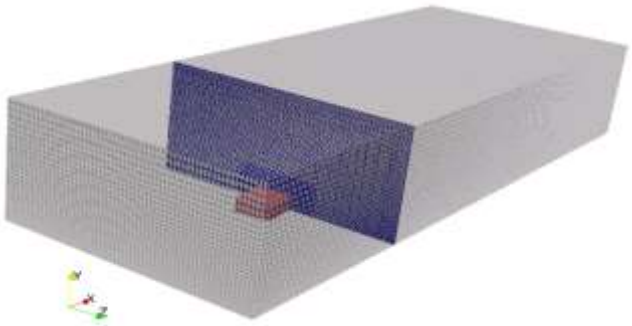

Fig. 11 A general view of the 3D domain and the building surrounded by a refined mesh region obtained using snappyHexMesh with 768,000 cells

regarding the procedure to create a high quality structured mesh using SnappyHexMesh utility in OpenFOAM can be found in a comprehensive tutorial in Jackson (2017).

After creating the mesh file, appropriate boundary conditions were assigned as shown in Fig. 10. For instance, the boundary condition of the inlet is "velocity inlet", the sides, and top are "symmetry", outlet is "outflow", and the building surfaces and the ground are "no-slip wall", where the tangential velocity component is set to zero. Implementing the "symmetry" boundary condition for the top of the domain will expedite the simulation; and because the top boundary is far enough from the building roof, this simplified assumption is believed to have no negative impact on the solution results.

In order to check the adequacy of grid resolution and make sure that the CFD simulation results do not depend on the grid size, the computational domain is discretized into four different grid sizes, as are listed in Table 6. The four mesh cases in Table 6 were run in ANSYS FLUENT and the time history of non-dimensional drag (cd) and lift coefficients (cl) over the total areas of building were monitored and used for the grid sensitivity analysis. Eventually, the mesh case 2 with 768,000 cells was selected as the main computational mesh for further CFD LES investigation in this study due to its good representation of the fine mesh and at the same time significant saving in computational costs in compare with case 4. The mesh case with 768,000 cells can be seen in Fig. 11. Fig. 12 also shows a 2D transverse section of the domain and building surrounded by the refined mesh region. Fig. 13 also shows a close view of the building model in ANSYS FLUENT. In Fig. 13, there are 90 monitoring points defined on the roof of low-rise building to record the time histories of pressure at each point.

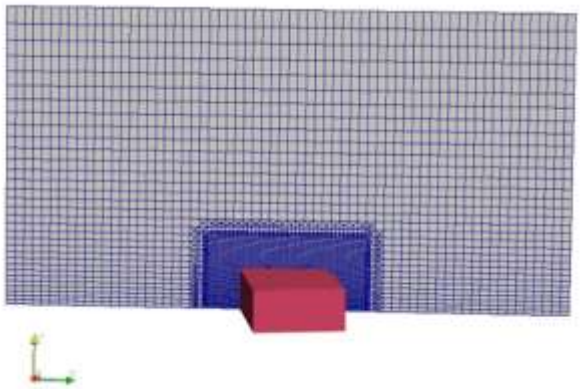

Fig. 12 A 2D transverse section of the domain and the low-rise building model surrounded by a refined mesh region obtained using snappyHexMesh with 768,000 cells

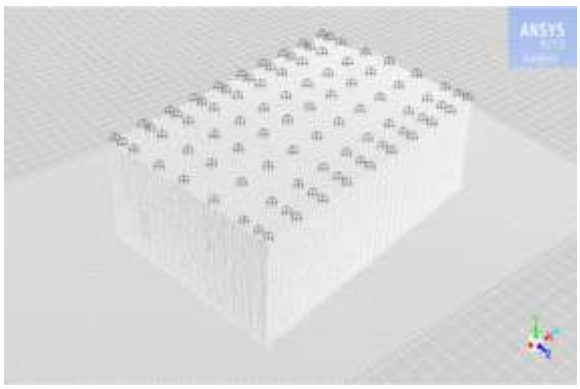

Fig. 13 The 90 monitoring points defined on the roof of low-rise building in CFD model to record time histories of pressure at each points

Running CFD cases using Large Eddy Simulation (LES) closure

Similar to the empty domain case, in order to generate the fluctuating wind velocity at inlet appropriate for LES simulation and creating target turbulence content suitable for ABL condition, first, a UDF is written to simulate the mean wind speed profile according to the log-law profile (Holmes 2015). Afterwards, vortex method was utilized to consider the inflow wind velocity fluctuations. The two recommended sets of variables for inputs are (1) TI = 25% and TLS = 10 m for building model at location 3 and 7, and (2) TI = 30% and TLS = 15 m for building model at location 7. The LES turbulence closure was run for both cases. More details regarding the LES and solver settings are presented as follows.

In ANSYS FLUENT, for the subgrid-scale model, Smagorinsky-Lilly was implemented. The pressure-based algorithm was employed. In the solution method's box, Semi-Implicit Method for Pressure-Linked Equations (SIMPLE) scheme has been applied to the pressure-velocity coupling. For the spatial discretization, least squares cell-based option was selected for the gradient, and for pressure a second order discretization was used. The time step was calculated based on the requirement of the Courant–Friedrich–Lewy (CFL) number to be less than unity to avoid the numerical instability

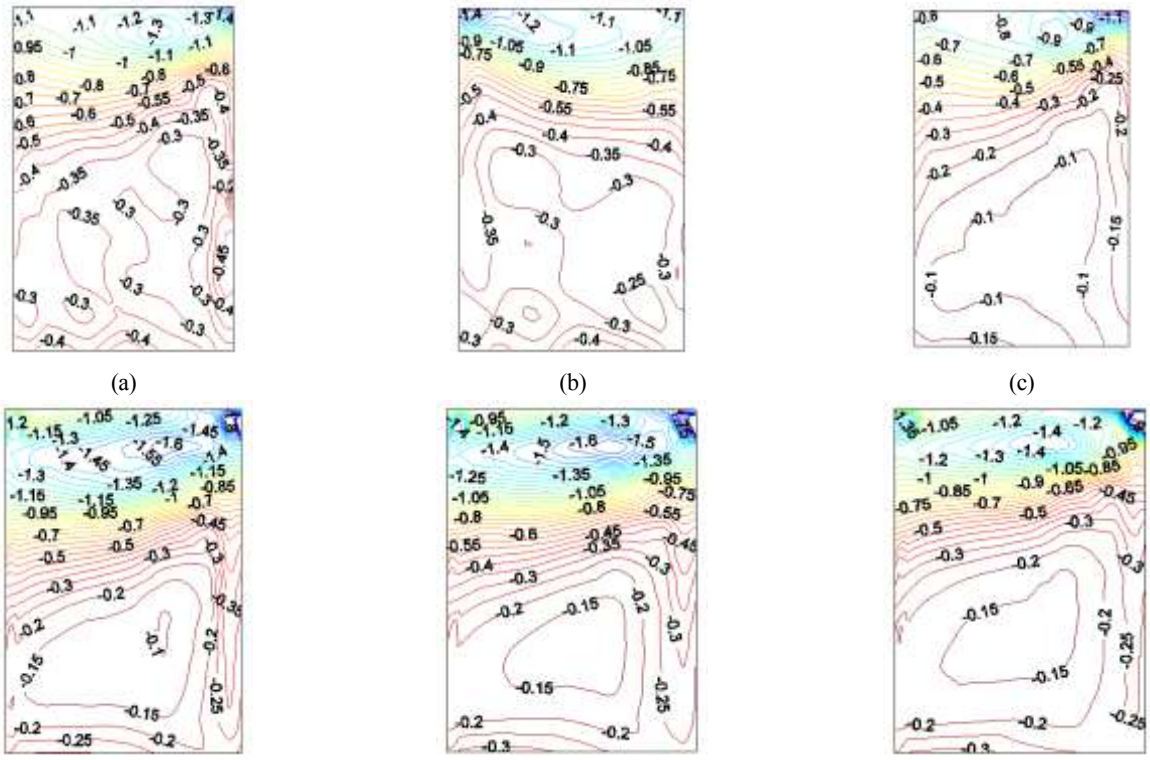

(a) (b) (c)

(d) (e) (f)

Fig. 14 Comparison of mean surface pressure coefficients (a) Full scale TTU field data (R279); (b) Full scale TTU field data (R1912); (c) model scale wind tunnel from NIST/UWO database; (d) CFD LES at location 7 (TI = 25%, TLS = 10 m); (e) CFD LES at location 7 (TI = 30%, TLS = 15 m); (f) CFD LES at location 3 (TI = 25%, TLS = 10 m)

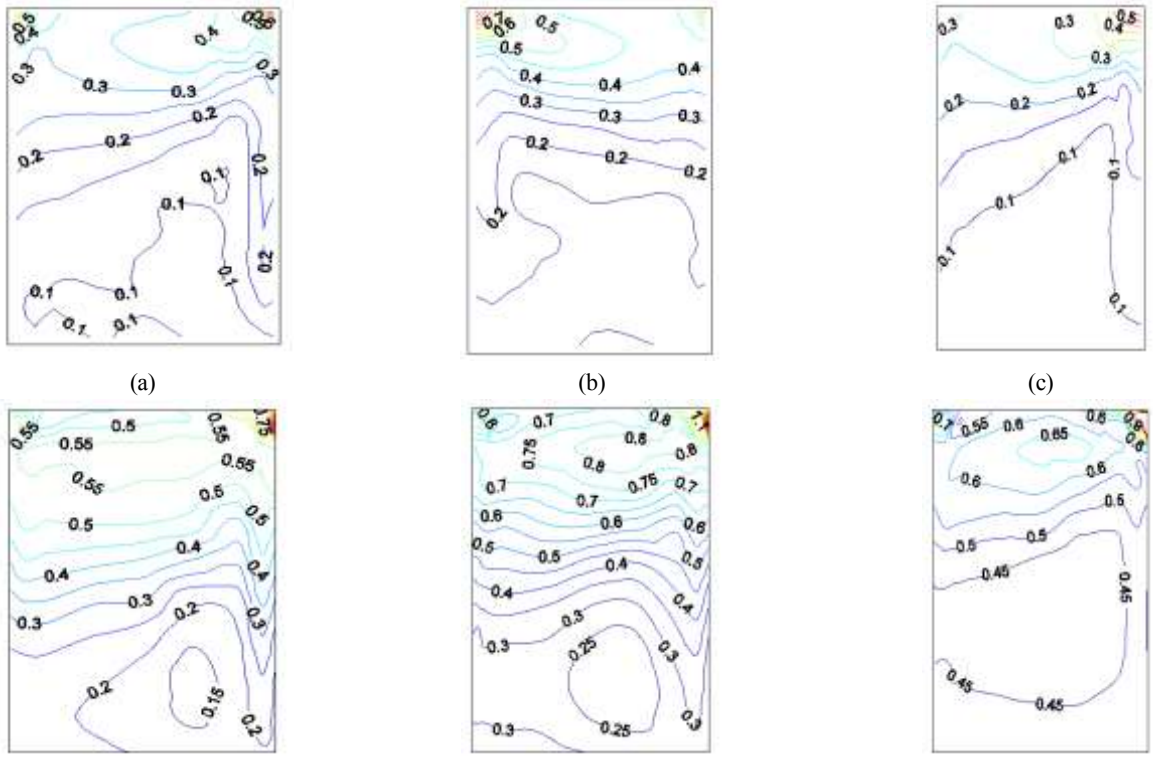

(a) (b) (c)

(d) (e) (f)

Fig. 15 Comparison of standard deviation surface pressure coefficients (a) Full scale TTU field data (R279); (b) Full scale TTU field data (R1912); (c) model scale wind tunnel from NIST/UWO database; (d) CFD LES at location 7 (TI = 25%, TLS = 10 m); (e) CFD LES at location 7 (TI = 30%, TLS = 15 m); (f) CFD LES at location 3 (TI = 25%, TLS = 10 m)

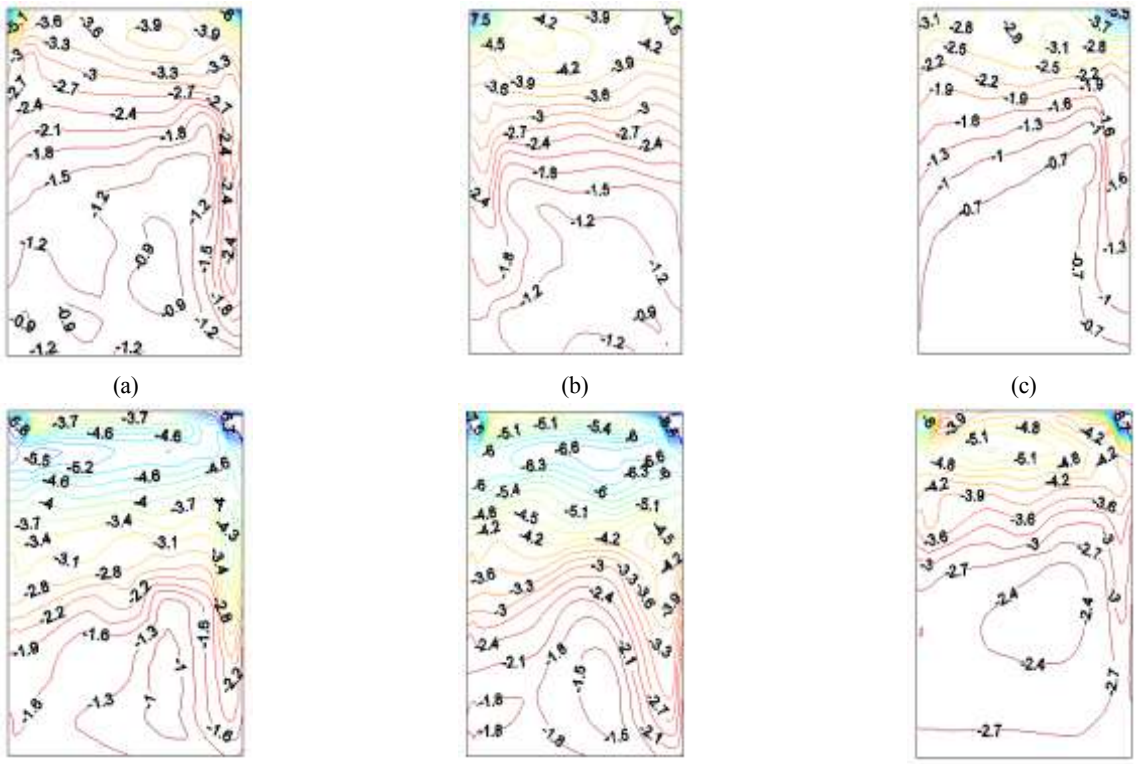

(a) (b) (c)

(d) (e) (f)

Fig. 16 Comparison of minimum 95% surface pressure coefficients (a) Full scale TTU field data (R279); (b) Full scale TTU field data (R1912); (c) model scale wind tunnel from NIST/UWO database; (d) CFD LES at location 7 (TI = 25%, TLS = 10 m); (e) CFD LES at location 7 (TI = 30%, TLS = 15 m); (f) CFD LES at location 3 (TI = 25%, TLS = 10 m)

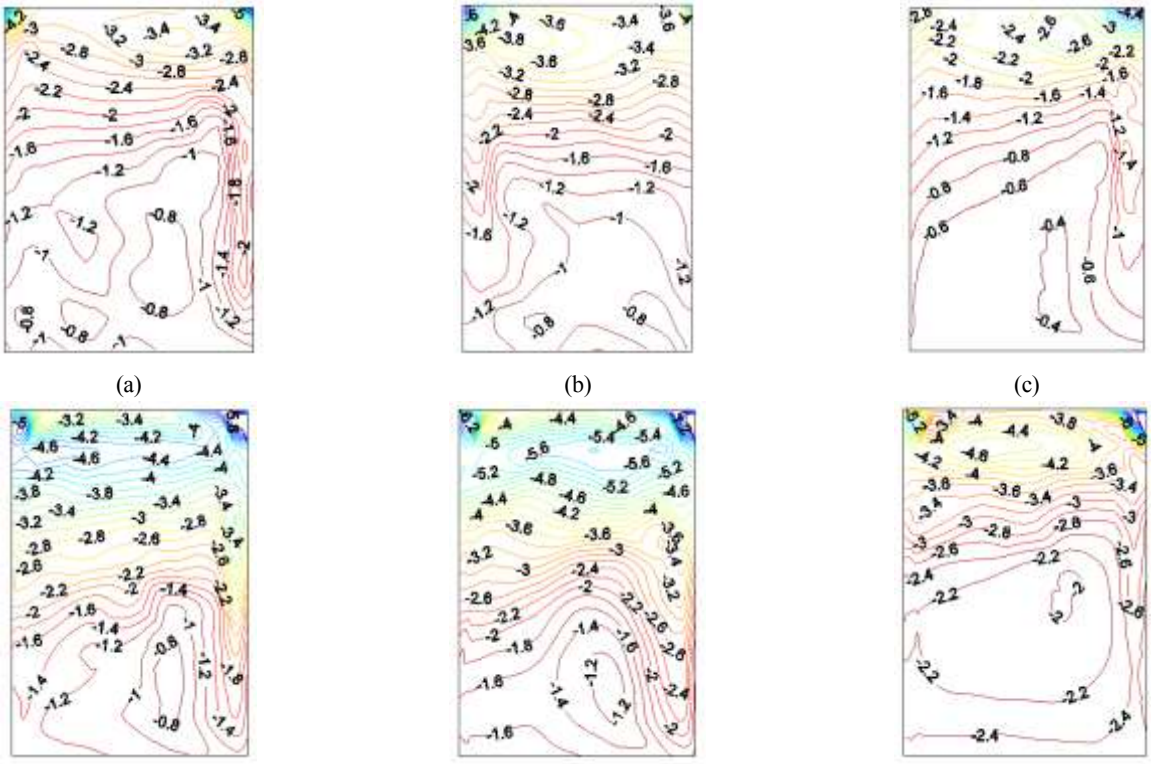

(a) (b) (c)

(d) (e) (f)

Fig. 17 Comparison of minimum 50% surface pressure coefficients (a) Full scale TTU field data (R279); (b) Full scale TTU field data (R1912); (c) model scale wind tunnel from NIST/UWO database; (d) CFD LES at location 7 (TI = 25%, TLS = 10 m); (e) CFD LES at location 7 (TI = 30%, TLS = 15 m); (f) CFD LES at location 3 (TI = 25%, TLS = 10 m)

that is $CFL \equiv \otimes t.V_H / min(dx, dy, dz) \leq 1$, whereis the time step, V_H is the local flow velocity, and *dx , dy , dz* are the cell dimensions. In addition, this time step is in accordance with the 30 Hz frequency of acquisition for the velocity and pressure measurements for the TTU filed data. The residual values for momentum and continuity are set as 10-8 and 10-6, respectively.

For each computational case, a job was submitted to the LSU High Performance Computing (HPC) clusters (LSU_HPC 2017). The processors on the SuperMike-II workq's compute nodes are Intel Xeon E5 2670 at the base frequency of 2.60 GHz. The processors are basically Xeon Sandy Bridge processors. The submitted job utilized 1 node and 16 parallel processors with a physical wall time of 96 hours to complete the simulation representing 15 min in full-scale. In the next sections, the CFD LES results for the mean and peak non-dimensional pressure distribution over the roof surface will be compared with TTU full-scale field measurements and small scale NIST/UWO wind tunnel testing data.

8. Results of CFD LES for low-rise building model

In this section, LES via vortex method was utilized to investigate the inflow wind velocity fluctuations in the pressure distribution over the roof surface of TTU full-scale building. In total, the results of three CFD LES cases are presented in this section as follows:

(1) CFD LES at location 7 (TI = 25%, TLS = 10 m);
(2) CFD LES at location 7 (TI = 30%, TLS = 15 m);
(3) CFD LES at location 3 (TI = 25%, TLS = 10 m).

The results of mean and peak pressure distribution over the roof surface for each case are compared with full-scale field measurements and wind tunnel data within the next sub-sections accordingly.

Comparison of mean and peak pressure coefficients

Fig. 14 represents the counters of mean surface pressure coefficients for full-scale CFD LES models versus two cases from full-scale TTU field data (R279 and R1912), and a small-scale model of the same benchmark building from NIST/UWO wind tunnel testing. It is worth noting that the wind angle for TTU R279 is 9.67° and the same wind angle was considered for the CFD LES model. However, the wind angle for the R1912 is 351.72° (-8.28°) with negligible difference from TTU R279 in symmetry to the longitudinal axis on roof. The wind angle for NIST/UWO wind tunnel data is 10º. Figure 14 shows that the roof mean pressure contour of a full-scale building simulated by the developed CFD LES models are better matched to the TTU field measurements than the small scale wind tunnel data. This proves that CFD can be utilized for appropriate estimation of mean pressure distribution on low-rise buildings with no scale issue if an accurate turbulence closure (LES) and inlet velocity fluctuations (vortex method) with tuned parameters are implemented within the numerical model.

Fig. 15 through Fig. 17 represent the standard deviation, the minimum 95% quantile peak pressure coefficients, and the minimum 50% quantile peak pressure coefficients for the full-scale CFD LES models versus full-scale TTU field data, and a small scale model from NIST/UWO wind tunnel testing. According to the Fig. 15(d), the standard deviation of CFD LES model 1 is better matched with full-scale TTU field measurements specifically in windward edge and corners rather than the small scale wind tunnel data from NIST/UWO.

According to Figs. 16 and 17, the results show that the roof peak pressure contours of a full-scale building simulated by the developed CFD LES model 1 at location 7 with input parameters of TI = 25%, and TLS = 10 m are very similar to the TTU full-scale field measurements. This is again another proof that if an accurate turbulence closure, like LES, and appropriate inlet velocity fluctuations (for instance using the vortex method with tuned input parameters) are implemented in CFD, the numerical model can be utilized for appropriate estimation of the peak and standard deviation of pressure distributions on low-rise buildings within the numerical model. In addition, in all three CFD LES models, high negative pressure values (suction effects) were observed near the corner and edges on the windward side of the roof similar to the TTU field data which are the spots on the roofthat separation bubbles start developing in a fluctuating manner. Identifying the extend of these regions will help to design appropriate mitigation features for surpassing the high suctions at corners and edges of the roof. Figs. 16(c) and 17(c) show that reproducing peak pressures in wind-tunnel is, however, a big challenge due to its limitation to correctly reproduce important flow characteristics and inherent scale issue with testing at large scales.

Comparison of correlation coefficients

To determine how the pressure coefficients are correlated across the roof surface, correlation coefficients for each pressure tap were calculated by considering a reference pressure tap (tap 5140 in TTU report). Fig. 18 represents the counters of correlation coefficient for full-scale CFD LES models versus full-scale TTU field data, and a small-scale model of the same benchmark building from NIST/UWO wind tunnel testing. The results show that the spatial correlation of the wind pressure coefficients based on the CFD LES at location 3 (TI = 25%, TLS = 10 m) represented in Fig. 18(f), is better reproduced in compare with the measured data in natural wind in full-scale. In addition, a low correlation can be observed after a short distance from the reference point until the middle of the roof, and after that, the correlation coefficients are increasing toward the leeward edge of the roof. This pattern gives an insight on how the flow de-attachment and attachment, and the separation bubble length can affect the correlation of pressures on various parts of the roof surface. However, for the two other CFD LES cases at location 7, Fig. 18(d) and I, it is noticeable that in 1/3 of the roof area in leeward, negative correlations are resulted. It means that in those areas, the time histories of pressure coefficients are changing in an opposite manner of the reference point measurement at tap 5140, i.e., an incensement in a reference variable in time history results in a reduction in other variables and vice versa. This is a very important observation that how the correlation of pressure measurements on the roof of low-rise buildings are sensitive to the proximity of the inlet boundary in CFD LES. Accordingly, it can be concluded that placing the low-rise building model at location 7 in CFD LES will result in an unrealistic correlation on the roof in compare

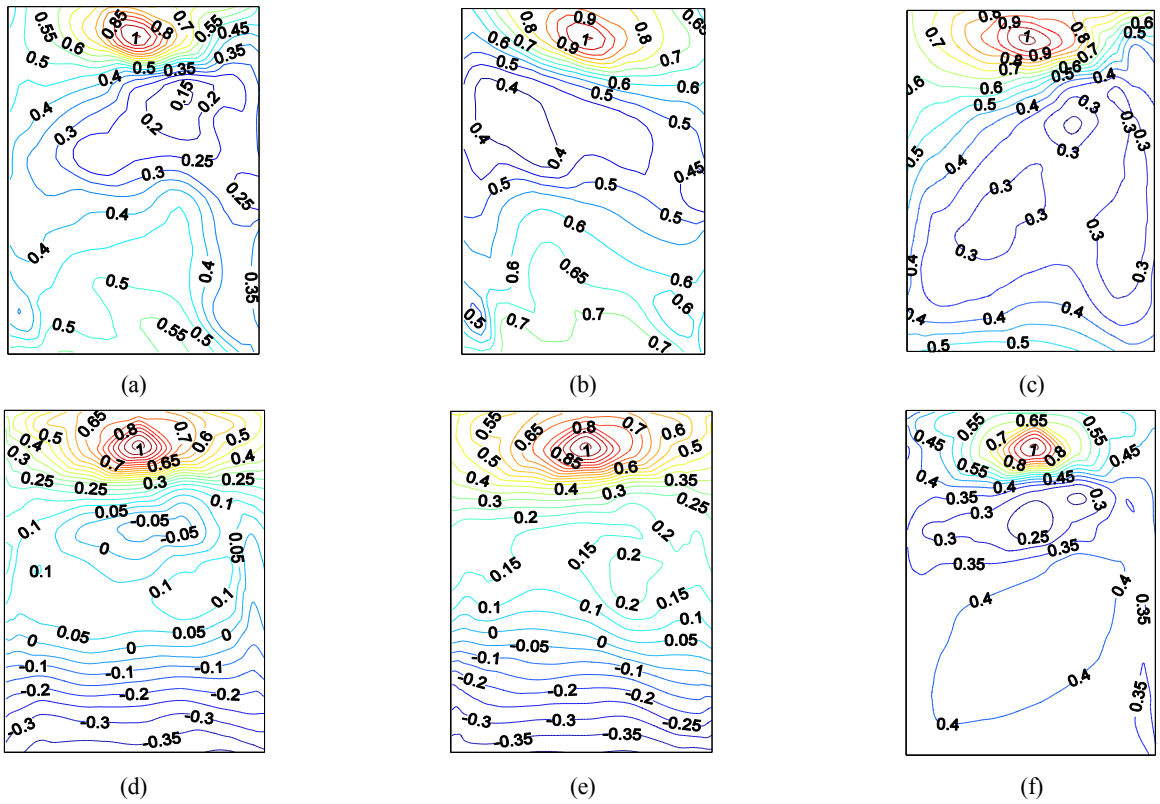

Fig. 18 Comparison of the correlation contours (a) Full scale TTU field data (R279); (b) Full scale TTU field data (R1912); (c) model scale wind tunnel from NIST/UWO database; (d) CFD LES at location 7 (TI = 25%, TLS = 10 m); (e) CFD LES at location 7 (TI = 30%, TLS = 15 m); (f) CFD LES at location 3 (TI = 25%, TLS = 10 m)

with the field measurements, and location 3 is a better representation of real world scenario.

Finally, it should be noted that these comparisons are based on calculations of correlation coefficients in compare to one reference tap, averaged over all frequency ranges. However, within the next sections, Proper Orthogonal Decomposition (POD) technique is used to analyze the spatial correlation matrix of fluctuating wind pressures between every two pressure taps at various locations over the roof surface.

In order to quantify the differences of peak pressure values over the roof surfaces for different cases shown in Fig. 16, a comparison is made within the next section between the external pressure coefficients, GCp, for roof components and cladding (C&C) suggested by ASCE 7-10, and the CFD LES versus wind-tunnel data and TTU field measurements.

9. Comparisons of simulated results with ASCE 7-10

The procedure outlined in ASCE 7-10 to calculate external pressure coefficients, GCp, for roof components and cladding (C&C) will be described, and the CFD LES results will be compared with the GCp recommended design values from ASCE 7-10 along with wind-tunnel data and TTU field measurements. According to the ASCE 7-10, the external pressure coefficients recommended for C&C for gable roof of low-rise buildings with a roof pitch less than 7° shall be evaluated based on surface zone definition in figure 30.4-2A from ASCE 7-10 (ASCE7-2010 2010). According to ASCE 7-10, the first step to evaluate GCp is to calculate the effective width, α, and defining the effective area of each zone on the roof. For the case study TTU low-rise building with dimensions of 3.96 m x 9.14 m x 13.72 m, the value of is calculated as follows

$$\alpha = \min\{0.1 \text{ x } 9.14, 0.4 \text{ x } 3.96\} = 0.914 \text{ m} > \max\{0.9 \text{ m}, 0.04 \text{ x } 9.14 = 0.9 \text{ m}\} \quad (10)$$

According to ASCE 7-10, a gust factor of G, should be multiplied to the measured peak pressure coefficients to calculate the counterparts code-specified GCp values. According to section 26.9.4 in ASCE 7-10, the gust-effect factor for a rigid building shall be taken as 0.85 or calculated from a formula (26.9-6) in the code as follows

$$G = 0.925\left(\frac{1 + 1.7 g_Q I_{\bar{z}} Q}{1 + 1.7 g_v I_{\bar{z}}}\right) \quad (11)$$

$$I_{\bar{z}} = c\left(\frac{10}{\bar{z}}\right)^{1/6} \quad (12)$$

where I $\bar{}$Z is the intensity of turbulence at height $\bar{}$Z which is equivalent to 0.6 h, but not less than Zmin for all building heights. h is the mean roof height. gQ and gv should be considered as 3.4. The background response Q is given by

$$Q = \sqrt{\frac{1}{1 + 0.63\left(\frac{B + h}{L_{\bar{z}}}\right)^{0.63}}} \quad (13)$$

Table 7 The parameters used to estimate gust factor in this study for TTU building

h (m)	B (m)	$\bar{Z}$ (m)	$\bar{\varepsilon}$	c	l (m)	$\mathbf{I_z}$	$\mathbf{L_z}$ (m)	Q	G
3.96	9.14	4.57	1/5	0.2	152.4	0.23	130.31	0.93	0.89

Table 1. Finally, the gust factor was calculated as 0.89.

In order to comprehensively evaluate the procedure defined

Table 8 A comparison of GCp for C&C in ASCE 7-10, and corresponding TTU field data, NIST/UWO wind tunnel measurements, CFD LES simulations, and LSU open-jet testing

Zone labels	Effective area (m^2)	*GCp*								
		ASCE (Figure 30.4-2A)	TTU (R279) at 9.67º	TTU all directions	NIST/UWO 10º	NIST/UWO at 0º,10º,45º,90º	Open Jet at 0º ,90º	CFD LES 1	CFD LES 2	CFD LES 3
1a	43.52	-0.9	-0.54	-0.66	-0.28	-0.28	-0.58	-0.59	-0.80	-1.78
1b	43.52	-0.9	-0.50	-1.11	-0.24	-0.65	-1.04	-0.63	-0.90	-1.79
2a	3.34	-1.43	-1.44	-2.34	-0.86	-0.86	-1.37	-1.57	-2.21	-2.70
2b	3.34	-1.43	-1.87	-2.08	-1.16	-1.21	-1.53	-2.50	-3.06	-3.41
2c	10.87	-1.1	-0.61	-1.32	-0.33	-0.33	-0.53	-0.66	-0.90	-1.85
2d	10.87	-1.1	-0.88	-1.59	-0.41	-0.87	-1.22	-0.94	-1.32	-1.89
2e	3.34	-1.43	-0.50	-1.05	-0.19	-0.38	-0.85	-0.69	-0.98	-2.13
2f	3.34	-1.43	-0.45	-1.43	-0.17	-0.69	-1.53	-0.59	-0.86	-2.09
3a	0.83	-2.8	-3.58	-4.75	-1.21	-1.25	-2.30	-1.81	-2.73	-3.05
3b	0.83	-2.8	-4.62	-4.62	-2.05	-2.05	-3.53	-2.60	-3.49	-4.64
3c	0.83	-2.8	-0.49	-2.57	-0.22	-0.30	-0.76	-0.76	-1.05	-2.14
3d	0.83	-2.8	-0.41	-2.06	-0.21	-1.25	-3.26	-0.64	-0.91	-2.08

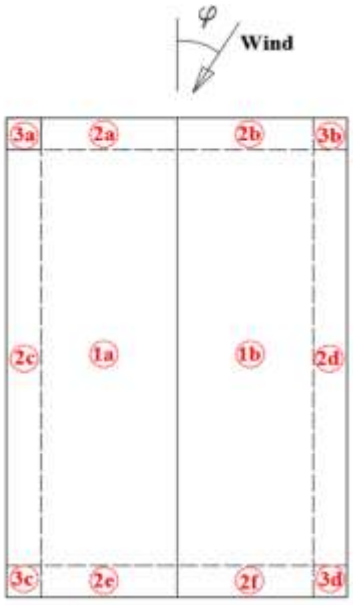

Fig. 19 New definition of zones on the roof of low-rise building for a comparison of *GCp* with ASCE 7-10 recommended values

where B is the horizontal dimension, and stands for the integral length scale of turbulence at $0.6h$ height. L_z can be estimated by using the following formula

$$L_{\bar{z}} = l\left(\frac{\bar{z}}{10}\right)^{\bar{\varepsilon}} \tag{14}$$

Where $\boldsymbol{l}$ and $\bar{\varepsilon}$ are constants listed in Table 26.9-1 in ASCE 7-10. The parameters used to estimate gust factor are listed in Table 1. Finally, the gust factor was calculated as 0.89.

In order to comprehensively evaluate the procedure defined by ASCE 7-10, new subdivisions are defined for each zone on the roof surface as can be seen in Fig. 19, and the corresponding GCp are calculated for each zone and presented in Table 8 for CFD LES, NIST/UWO wind tunnel data, TTU field measurements, and open-jet testing. However, because the pressure coefficients recommended by ASCE 7-10 are based on the 3 seconds gust speeds, the time history of pressure from experimental measurements and CFD LES should be re-evaluated to be consistent with the approach adopted by the code. In the next section, the procedure to extract peak values according to 3 seconds gust wind speed will be described.

Estimation of peak pressures over 3 seconds

As described earlier, the pressure coefficients recommended by ASCE 7-10 are based on the 3 seconds (3-s) gust speeds, and therefore the time histories of pressure data from the field, experimental measurements, and CFD LES should be re-analysis to reflect the 3-s gust speed approach adopted by the code. For the TTU field data and CFD LES, the time history of 15 min wind velocity and pressure data at full-scale were available. Therefore, the three seconds (3-s) wind velocity was calculated by dividing the time history of velocity into several windows, each one with a length of 3 seconds. The mean value for each window was calculated, and then the maximum of calculated mean values was specified as the 3-s wind velocity. The non-dimensional pressure coefficients were calculated based on the new 3-s wind velocity, accordingly.

$$C_p'(t) = \frac{p(t) - \bar{p}_s}{(1/2)\rho {U_{3-s}}^2} \tag{15}$$

After calculating the new time history, C $'_p(t)$, the peak pressure values should be evaluated. Since peak pressure is

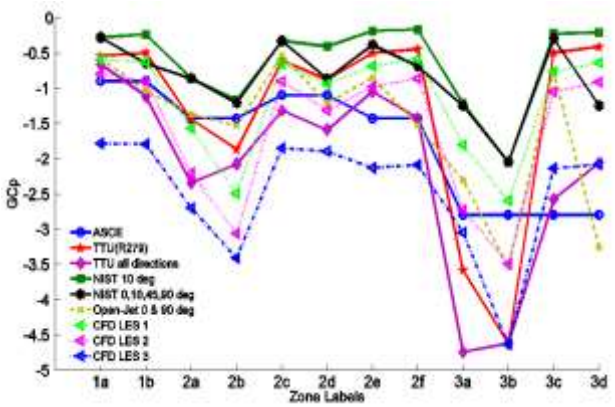

Fig. 20 A comparison of *GCp* values defined by ASCE 7-10, and corresponding calculated values from TTU full-scale field, open-jet testing, NIST/UWO wind tunnel data, and CFD LES simulations

a random variable, it is not possible to get the same value for peak pressures in different records while having the same mean value (Simiu 2011). Sadek and Simiu (Sadek and Simiu 2002) investigated the influence of the time-series duration and sampling frequency on the estimated peaks of input time series. To develop the procedure, the appropriate marginal probability distribution of the time series using the probability plot correlation coefficient method was identified and then used to estimate the distribution of the peaks by implementing the standard translation processes approach. They showed that the peaks estimated by the proposed procedure are less dependent than observed peaks on record length and sampling rates. In this study, the peak values are extracted from the time series at each tap locations by using the approach introduced in Ref. (Sadek and Simiu 2002). A MATLAB function for computing of quantiles (i.e., values corresponding to specified probabilities of non-exceedance) of the maximum and minimum values of the input time series was developed by NIST which is accessible on the NIST website (Main 2011). The function of "maxminqnt" is called within MATLAB as follows

```
[max_qnt, min_qnt]
= maxminqnt (X, dur_ratio, CDF_qnt)
```
(16)

This function was used to calculate 95% peak quantile of the maximum (max_qnt) and minimum (min_qnt) values of time series of pressure coefficients. In the function, first input argument, "X", stands for the time history of pressure data, and there is an input argument "dur_ratio" to define the ratio of the duration for which peaks are required to the duration of the time series. In this study for calculating the 95% peak quantile for 1 hour (60 min), while having a 15 min data for TTU and CFD LES, a value of 60/15 = 4 was used for "dur_ratio". And for "CDF_qnt" a value of 0.95 was considered to calculate 95% peak quantiles.

For the 1:15 scaled model testing in LSU open-jet facility, the wind velocity and pressure data were measured for 9 min duration corresponding to 1-hour duration in prototype case.

Therefore, first the 3-s wind gust speed was identified by defining the 3 seconds window approach, and after producing the new time history of pressure data, a value of 1 was used for "dur_ratio". For NIST/UWO wind tunnel data, only pressure data for 38.4 min (2304 s) duration was available, and there was no time history of wind velocity. In that case, first the 3-s gust speed was estimated according to the durst curve (figure C26.5-1 from ASCE 7-10), and the non-dimensional pressure data corresponding to 38.4 min duration were divided by the square of the velocity ratio V_3 / V_{2304} based on the durst curve or (1.73/1.02)^2 = 2.88. Afterwards, the peak values of the new time history of pressure data were estimated by using the function "maxminqnt" in Eq. (16) and applying a value of 60/38.4 = 1.56 for the "dur_ratio" as an input. Finally, the evaluated 95% peak quantiles in all cases were multiplied by the gust factor of 0.89 for a comparison with GCp values defined in ASCE 7-10. The results are listed in Table 8, and represented also in Fig. 20.

By looking at Fig. 20, it is noticeable that ASCE7-10 significantly underestimates GCp for the studied model of low-rise building. The calculated GCp from TTU filed measurements is up to -4.75 which is around 1.7 times larger than the code-specified value of -2.8 for zone 3a at the corner of the roof. This large underestimation of the recommended values by ASCE 7-10 is believed to be mainly attributed to the fact that code-specified values are based on the published wind tunnel data. However, wind tunnel is not capable to fully simulate the ABL winds and reproduce the peak values of pressures. This fact can be observed in Fig. 20 by comparing the results of NIST/UWO wind tunnel data with code-specified values. In addition, open-jet testing measurements are showing a better agreement with ASCE 7-10 values than the NIST/UWO wind tunnel data. This proves another advantage of testing at large scale in open-jet facility. Finally, the CFD LES results are even better matched with TTU field values than the open-jet results. Therefore, it can be concluded that a full-scale CFD model of low-rise building with LES turbulence closure and an appropriate method for generating inflow velocity fluctuation at inlet boundaries could be utilized as a promising alternative to be implemented for design of roof components and cladding in low-rise buildings.

10. Proper Orthogonal Decomposition (POD) of measured wind pressure field

Proper Orthogonal Decomposition (POD) is a useful technique for analyzing random data by deriving the most efficient coordinate system (Tamura *et al.* 1999). The decomposition of the spatial correlation matrix of fluctuating wind pressure can be written as

$$[R_p][\Phi] = [\lambda][\Phi] \tag{17}$$

where [Rp] is the spatial correlation coefficient matrix of fluctuating wind pressure, [Φ] is the eigenvector matrix, and [λ] is the eigenvalue matrix. [Rp] which is an M*M square matrix whose elements are the correlation coefficients of fluctuating wind pressure between every two points, can be written as

$$[R_p] = \begin{bmatrix} R(p_1,p_1) & R(p_1,p_2) & \dots & R(p_1,p_n) \\ R(p_2,p_1) & R(p_2,p_2) & \cdots & R(p_2,p_n) \\ \vdots & \vdots & \vdots & \vdots \\ R(p_n,p_1) & R(p_n,p_2) & \cdots & R(p_n,p_n) \end{bmatrix} \tag{18}$$

Table 9 Eigenvalues, contribution proportions, and cumulative contribution proportions for the pressure field on TTU, CFD LES, and NIST/UWO model (without considering mean values)

	TTU full-scale field data (R279)			TTU full-scale field data (R1912)			CFD LES 1			CFD LES 2			CFD LES 3			NIST/UWO wind tunnel data		
Mode	Eigenvalue	Contribution proportion (%)	Cumulative contribution proportion (%)	Eigenvalue	Contribution proportion (%)	Cumulative contribution proportion (%)	Eigenvalue	Contribution proportion (%)	Cumulative contribution proportion (%)	Eigenvalue	Contribution proportion (%)	Cumulative contribution proportion (%)	Eigenvalue	Contribution proportion (%)	Cumulative contribution proportion (%)	Eigenvalue	Contribution proportion (%)	Cumulative contribution proportion (%)
1st	33.14	36.83	36.83	47.28	52.53	52.53	19.63	21.82	21.82	24.74	27.50	27.50	52.61	58.46	58.46	36.58	40.66	40.66
2nd	8.96	9.96	46.78	8.07	8.97	61.50	7.75	8.61	30.43	10.08	11.20	38.70	6.06	6.74	65.20	10.05	11.17	51.82
3rd	3.45	3.84	50.62	4.25	4.72	66.22	5.52	6.13	36.57	5.58	6.20	44.89	4.98	5.53	70.73	4.87	5.41	57.23
4th	3.22	3.57	54.19	3.38	3.75	69.97	4.40	4.90	41.46	4.33	4.82	49.71	2.98	3.31	74.04	3.39	3.76	61.00
5th	2.54	2.82	57.02	1.90	2.11	72.08	3.99	4.43	45.89	3.77	4.19	53.90	2.16	2.40	76.45	2.87	3.19	64.19
6th	2.02	2.25	59.26	1.35	1.50	73.58	3.04	3.38	49.28	3.19	3.55	57.45	1.75	1.95	78.39	2.65	2.95	67.14
7th	1.76	1.95	61.22	1.18	1.31	74.89	2.96	3.30	52.57	2.53	2.81	60.26	1.41	1.57	79.96	1.93	2.14	69.28
8th	1.71	1.90	63.12	1.09	1.21	76.10	2.61	2.90	55.48	2.31	2.57	62.83	1.22	1.36	81.32	1.58	1.75	71.03
9th	1.37	1.52	64.64	0.94	1.04	77.14	2.10	2.34	57.81	2.14	2.37	65.20	1.09	1.21	82.53	1.40	1.56	72.59
10th	1.23	1.36	66.01	0.93	1.04	78.18	2.04	2.27	60.08	1.92	2.13	67.33	1.00	1.11	83.64	1.18	1.32	73.90
20th	0.69	0.77	76.07	0.49	0.54	85.05	0.98	1.09	75.07	0.87	0.97	80.22	0.41	0.46	90.33	0.58	0.64	82.81
50th	0.32	0.36	91.03	0.19	0.22	94.81	0.31	0.34	93.37	0.23	0.25	95.11	0.11	0.12	97.82	0.22	0.25	94.23
70th	0.21	0.24	96.73	0.12	0.13	98.18	0.14	0.15	98.13	0.10	0.11	98.72	0.05	0.05	99.45	0.14	0.15	98.00
90th	0.00	0.00	100.00	0.00	0.00	0.00	0.00	0.00	0.00	0.00	0.00	0.00	0.00	0.00	0.00	0.00	0.00	100.00

The solutions for eigenvalues should be arranged in a descending order as: $\lambda_1 > \lambda_2 > \ldots > \lambda_n = 0$. The corresponding eigenvectors should be relocated accordingly.

In this section, the results of the POD analysis on the pressure coefficient data from TTU full-scale field data, CFD LES, and NIST/UWO model for wind attack angle of $\approx 10°$ are presented. It is worth noting that in each case, according to (Tamura *et al*. 1999), the mean value was removed from the time history of pressure coefficients; then, the eigenvalue decomposition was applied on the spatial correlation matrix in order to obtain eigenvalues and the corresponding eigenvectors. Table 9 represents the POD analysis results for spatial correlation matrix of fluctuating wind pressures on TTU full-scale field data, CFD LES, and NIST/UWO model.

As can be seen in Table 9 the contribution proportions of each mode to the global wind pressures field are significant within the few first modes, while there are 90 modes in total for each case. In addition, the cumulative contribution proportion up to the 50th mode is about 91% to 98% when considering all six cases. It shows that the first several modes play a significant role to represent a fine detail of the global characteristics of wind fluctuation over the roof surface, while the other higher order modes are reproducing just the local distributions. In addition, for the CFD LES 3 and TTU (R1912), the contribution of the first 20 modes are higher in compare to the other cases. However, for the CFD LES 1 and CFD LES 2, lower values than the other cases can be observed. It proves again that how the distance from the inlet boundary in CFD simulation is affecting the spatial correlation of wind pressure measurements at various tap locations on the roof surface. Therefore, it is strongly recommended paying attention to the spatial correlation of wind when using LES by applying an appropriate longitudinal extension of the domain in front of the building model and the inflow boundary proximity in CFD simulations.

11. Conclusions

In this paper, CFD simulations with LES are executed on a TTU full-scale building model with appropriate inflow fluctuations to mimic peak pressures on the roof surfaces. The vortex method was employed to generate the inflow wind fluctuations at the inlet boundaries for representing the ABL wind characteristics and the full turbulence structure with both time and space correlations. The main conclusions are drawn as follows:

- According to the CFD results, LES with appropriate transient inlet generation technique can reproduce the mean pressure coefficients distribution on the roof of low-rise buildings consistent with full-scale field measurements;
- Peak pressures are well reproduced in LES and little discrepancy was observed in some spots on the roof. For instance, for CFD LES at location 7 (TI = 25%, TLS = 10 m), the minimum 95% peak pressure is -5.7 which shows a relative error of 11.76% regarding the corresponding -5.1 for TTU R279 at roof corner with high suction effect. However, the results of peak pressure simulation in this study are

very promising, because as concluded in (Janajreh and Emil 2012), it is still a challenge in the CFD LES to mimic peak pressures;

- This study suggests building location different from existing guidelines by COST and AIJ, as both recommendations are mainly based on RANS models and therefore not directly applicable to LES models.
- The results show that the ASCE 7-10 significantly underestimates *GCp* for C&C design. For instance, at zone 3a, the code-specified *GCp* is -2.8 with a 41% relative error in comparison with the -4.75 from TTU all directions. This significant underestimation is mainly attributed to the fact that code-specified values are based on the published wind tunnel data.
- The values of *GCp* for C&C design from open-jet testing measurements showed a better agreement with ASCE 7-10 specified values than the NIST/UWO wind tunnel data. This proves another advantage of testing at large scale in an open-jet facility which partially alleviates the scale issue in laboratory measurements;
- The values of *GCp* for C&C design from CFD LES 3 represent a conservative prediction of TTU full scale data for all directions. However, at zone with label 3b, the result of -4.64 for *GCp* shows a relative error of 2.32% in comparison with the -4.75 form TTU all directions at zone 3a;
- The results of a POD analysis on the pressure coefficient data showed how the distance from the inlet boundary in CFD LES simulations affects the detail of the global characteristics of wind fluctuation over the roof surface;
- High negative pressure values (suction effects) were observed in CFD LES at spots where separation bubbles start developing in a fluctuating manner. Identifying the extend of these regions will help to design appropriate mitigation features for surpassing the high suctions at these spots;
- With advances in digital data storage and High Performance Computing (HPC) technology via high speed enhanced CPUs, CFD with LES turbulence closure becomes a very promising approach for reproducing time histories of pressure data comparable to full-scale measurements.

Acknowledgements

This research is supported by the Louisiana Board of Regents (BoR) (Research Competitiveness Subprogram [RCS, LEQSF(2016-19)-RD-A-02] and Enhancement Program). Additional fund was received from the Office of Research & Economic Development, Louisiana State University (2017-18 Faculty Research Grant - Emerging Research), and the Louisiana Transportation Research Center (LTRC) (14-2TIRE, 14-1ST, and 16-4ST). The authors would like to thank Dr. Kishor Mehta, Dr. Douglas Smith, and Dr. Stephen Morse for generously sharing the field data related to the time-history of wind velocity and pressure measurements from the Wind Engineering Research Field Laboratory (WERFL) at Texas Tech University (TTU). The numerical part of this research was mainly conducted with High Performance Computing (HPC) resources on SuperMike-II clusters provided by Louisiana State University. The first author would like to thank AIR Worldwide company for its financial support to present this research in EMI 2018 conference at Massachusetts Institute of Technology (MIT), Cambridge, MA.

References

Aboshosha, H., Bitsuamlak, G. and El Damatty, A. (2015), "Turbulence characterization of downbursts using LES", *J. Wind Eng. Indust. Aerod*, **136**, 44-61. https://doi.org/10.1016/j.jweia.2014.10.020.

Aly, A.M. (2014), "Atmospheric boundary-layer simulation for the built environment: past, present and future", *Build. Environ*., **75**, 206-221. https://doi.org/10.1016/j.buildenv.2014.02.004.

Aly, A.M. (2016), "On the evaluation of wind loads on solar panels: The scale issue", *Solar Energy*, **135**, 423-434. https://doi.org/10.1016/j.solener.2016.06.018.

Aly, A.M. and Gol-Zaroudi, H. (2017), "Atmospheric boundary layer simulation in a new open-jet facility at LSU: CFD and experimental investigations", *Measurement*, **110**, 121-133. https://doi.org/10.1016/j.measurement.2017.06.027.

ASCE7-2010. (2010), *Minimum Design Loads for Buildings and Other Structures*, ASCE Standard, ASCE/SEI 7-10. American Society of Civil Engineers, Reston, Virginia, USA.

Bienkiewicz, B. and Ham, H. (2003), "Wind tunnel modeling of roof pressure and turbulence effects on the TTU test building", *Wind Struct., Int. J.*, **6**(2), 91-106. https://doi.org/10.12989/was.2003.6.2.091.

Davidson, L. (2007), "Using isotropic synthetic fluctuations as inlet boundary conditions for unsteady simulations", *Adv. Appl. Fluid Mech*., **1**(1), 1-35.

Davidson, L. (2008), "Hybrid LES-RANS: Inlet boundary conditions for flows with recirculation", *Proceedings of the 2007 Symposium of Hybrid RANS-LES Methods*, Corfu, Greece, June.

Dhunny, A.Z., Lollchund, M.R. and Rughooputh, S.D.D.V. (2015), "A high-resolution mapping of wind energy potentials for Mauritius using Computational Fluid Dynamics (CFD)", *Wind Struct., Int. J.*, **20**(4), 565-578. https://doi.org/10.12989/was.2015.20.4.565.

Feng, R., Liu, F., Cai, Q., Yang, G. and Leng, J. (2018), "Field measurements of wind pressure on an open roof during Typhoons HaiKui and SuLi", *Wind Struct., Int. J.*, **26**(1), 11-24. https://doi.org/10.12989/was.2018.26.1.011.

FLUENT. (2015), *FLUENT C.F.D.* ANSYS Inc., Canonsburg, Pennsylvania, USA, 15317.

Franke, J., Hellsten, A., Schlunzen, K.H. and Carissimo, B. (2011), "The COST 732 best practice guideline for CFD simulation of flows in the urban environment: a summary", *Int. J. Environ. Pollut*., **44**(1-4), 419-427. https://doi.org/10.1504/IJEP.2011.038443.

Gol-Zaroudi, H. and Aly, A.M. (2017), "Open-jet boundary-layer processes for aerodynamic testing of low-rise buildings", *Wind Struct., Int. J.*, **25**(3), 233-259. https://doi.org/10.12989/was.2017.25.3.233.

He, J., Pan, F. and Cai, C. (2017), "A review of wood-frame low-rise building performance study under hurricane winds", *Eng. Struct*., **141**, 512-529. https://doi.org/10.1016/j.engstruct.2017.03.036.

Ho, T.C.E., Surry, D. and Morrish, D.P. (2003), *NIST/TTU Cooperative Agreement—Windstorm Mitigation Initiative: Wind Tunnel Experiments on Generic Low Buildings*, BLWT-SS20-2003, Boundary-layer Wind Tunnel Laboratory, University of Western Ontario, London, Canada.

Højstrup, J., Larsen, S.E. and Madsen, P.H. (1990), "Power spectra of

horizontal wind components in the neutral atmospheric surface boundary layer," *Proceedings of the AMS 9th Symposium on Turbulence and Diffusion*, Roskilde, Denmark.
Holmes, J.D. (2015), *Wind Loading of Structures*, Taylor and Francis, New York, USA.
Jackson, A. (2017), "A comprehensive tour of snappy HexMesh", *Proceedings of the 7th OpenFOAM Workshop*, Berlin, Germany, October.
Janajreh, I. and Emil, S. (2012), "Large eddy simulation of wind loads on a low-rise structure and comparison with wind tunnel results", *Appl. Mech. Mater.*, **152**, 1806-1813. https://doi.org/10.4028/www.scientific.net/AMM.152154.1806.
Keating, A., Piomelli, U., Balaras, E. and Kaltenbach, H. (2004), "A priori and a posteriori tests of inflow conditions for large-eddy simulation", *Phys. Fluid.*, **16**(12), 4696-4712. https://doi.org/10.1063/1.1811672.
Kramlich, J. (1980), "The fate and behavior of fuel-sulfur in combustion systems", Ph.D. Dissertation; Washington State University, Washington, USA.
Levitan, M.L. and Mehta, K.C. (1992a), "Texas tech field experiments for wind loads part 1: building and pressure measuring system", *J. Wind Eng. Industr. Aerodyn.*, **43**(1-3), 1565-1576. https://doi.org/10.1016/0167-6105(92)90372-H.
Levitan, M.L. and Mehta, K.C. (1992b), "Texas tech field experiments for wind loads part II: meteorological instrumentation and terrain parameters", *J. Wind Eng. Industr. Aerodyn.*, **43**(1-3), 1577-1588. https://doi.org/10.1016/0167-6105(92)90373-I.
LSU_HPC. (2017), *High Performance Computing at Louisiana State University*, Louisiana State University.
Lumley, J.L. and Panofsky, H.A. (1964), The Structure of Atmospheric Turbulence. John Wiley and Sons, New York, USA.
Lund, T., Wu, X. and Squires, K. (1998), "Generation of turbulent inflow data for spatially-developing boundary layer simulations", *J. Comput. Phys.*, **140**(2), 233-258. https://doi.org/10.1006/jcph.1998.5882.
Main, J.A. (2011), "Special-purpose software: MATLAB functions for estimation of peaks from time series", National Institute of Standards and Technology, Maryland, USA.
Mann, J. (2012), *Atmospheric Turbulence*, Routledge, London, UK.
Mann, J., Kristensen, L. and Jensen, N.O. (1998), *Uncertainties of Extreme Winds, Spectra, and Coherences*, in *Bridge Aerodynamics*, Balkema Publishers, AA/Taylor and Francis, The Netherlands.
Mathey, F., Cokljat, D. and Bertoglio, J. (2006a), "Specification of LES inlet boundary condition using vortex method", *Prog. Comput. Fluid Dyn.*, **6**, 58-67. http://doi.org/10.1504/PCFD.2006.009483.
Mathey, F., Cokljat, D., Bertoglio, J.P. and Sergent, E. (2006b), "Assessment of the vortex method for large eddy simulation inlet conditions", *Prog. Comput. Fluid Dyn.*, **6**(1-3), 58-67.
Moret Rodrigues, A., Tome, A. and Gloria Gomes, M. (2017), "Computational study of the wind load on a free-form complex thin shell structure", *Wind Struct., Int. J.*, **25**(2), 177-193. https://doi.org/10.12989/was.2017.25.2.177.
Morrison, M., Brown, T. and Liu, Z. (2012), "Comparison of field and full-scale laboratory peak pressures at the IBHS research center", *Proceedings of the ATC/SEI Advances in Hurricane Engineering Conference*, Florida, USA. October.
Okada, H. and Ha, Y. (1992), "Comparison of wind tunnel and full-scale pressure measurement tests on the Texas Tech Building", *J. Wind Eng. Indust.,* **43**(1-3), 1601-1612. https://doi.org/10.1016/0167-6105(92)90375-K.
OpenFOAM (2015), *Openfoam User Guide*, OpenFOAM Foundation Ltd., e2888.
Ozdogan, M., Sungur, B., Namli, L. and Durmus, A. (2017), "Comparative study of turbulent flow around a bluff body by using two-and three-dimensional CFD", *Wind Struct., Int. J.*, **25**(6), 537-549. https://doi.org/10.12989/was.2017.25.6.537.
Sadek, F. and Simiu, E. (2002), "Peak non-Gaussian wind effects for database-Assisted low-rise building design", *J. Eng. Mech.*, **128**(5), 530-539. https://doi.org/10.1061/(ASCE)0733-9399(2002)128:5(530).
Sergent, E. (2002), "Vers une methodologie de couplage entre la Simulation des Grandes Echelles et les modeles statistiques", Ph.D. Dissertation; Ecole centrale de Lyon, Ecully, France.
Simiu, E. (2009), "Toward a standard on the wind tunnel method", NIST Technical Note, **1655**, 1-36.
Simiu, E. (2011), *Design of Buildings for Wind - A Guide for ASCE 7-10 Standard Users and Designers of Special Structures*, John Wiley and Sons Company, New York, USA.
Smirnov, A., Shi, S. and Celik, I. (2001), "Random Flow Generation Technique for Large Eddy Simulations and Particle-Dynamics Modeling", *J. Fluid Eng., Amer. Soc. Mech. Eng.*, **123**(2), 359. https://doi.org/10.1115/1.1369598.
Smith, D.A., Morse, S.M. and Mehta, K.C. (2017), *Wind Engineering Research Field Laboratory Selected Data Sets for Comparison to Model-Scale, Full-Scale and Computational Fluid Dynamics Simulation*s, Wind Science and Engineering Research Center, Texas Tech University, Lubbock, Texas, USA.
Tabor, G. and Baba-Ahmadi, M. (2010), "Inlet conditions for large eddy simulation: A review", *Comput. Fluid.*, **39**(4), 553-567. https://doi.org/10.1016/j.compfluid.2009.10.007.
Tamura, Y., Suganuma, S., Kikuchi, H. and Hibi, K. (1999), "Proper orthogonal decomposition of random wind pressure field", *J. Fluids Struct.*, **13**(7-8), 1069-1095. https://doi.org/10.1006/jfls.1999.0242.
Tieleman, H., Ge, Z., Hajj, M. and Reinhold, T. (2003), "Pressures on a surface-mounted rectangular prism under varying incident turbulence", *J. Wind Eng.*, **91**(9), 1095-1115. https://doi.org/10.1016/S0167-6105(03)00045-X.
Tominaga, Y., Mochida, A., Yoshie, R., Kataoka, H., Nozu, T., Yoshikawa, M. and Shirasawa, T. (2008), "AIJ guidelines for practical applications of CFD to pedestrian wind environment around buildings", *J. Wind Eng. Industr. Aerodyn.*, **96**(10), 1749-1761. https://doi.org/10.1016/j.jweia.2008.02.058.
VDI. (2005), *VDI 3783, Part 9, 2005. Environmental Meteorology-Prognostic Micro-Scale Windfield Models-Evaluation for Flow around Buildings and Obstacles*, Beuth Verlag GmbH, Berlin, Germany.
Xu, Y. (1995), "Model-and full-scale comparison of fatigue-related characteristics of wind pressures on the Texas Tech Building", *J. Wind Eng. Industr. Aerodyn.*, **58**(3), 147-173. https://doi.org/10.1016/0167-6105(95)00012-7.
Yousef, M.A.A., Selvam, P.R. and Prakash, J. (2018), "A comparison of the forces on dome and prism for straight and tornadic wind using CFD model", *Wind Struct., Int. J.*, **26**(6), 369-382. https://doi.org/10.12989/was.2018.26.6.369.
Zhang, X. (2009), *CFD Simulation of Neutral ABL Flows*, Risoe National Lab. for Sustainable Energy, Technical University of Denmark, Denmark.

AD